

DTIC FILE COPY

④

GL-TR-89-0196

AD-A216 641

Deterministic Modeling of Regional Waveforms  
From the Nevada Test Site

L.J. Burdick  
C.K. Saikia  
D.V. Helmberger

Woodward Clyde Consultants  
566 El Dorado Street  
Pasadena, CA 91101

19 July 1989

Final Report  
5 September 1988 - 5 March 1989

APPROVED FOR PUBLIC RELEASE; DISTRIBUTION UNLIMITED

GEOPHYSICS LABORATORY  
AIR FORCE SYSTEMS COMMAND  
UNITED STATES AIR FORCE  
HANSCOM AIR FORCE BASE, MASSACHUSETTS 01731-5000

DTIC  
ELECTE  
JAN 13 1990  
S E D

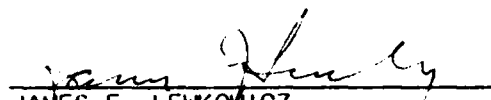
90 01 16 122

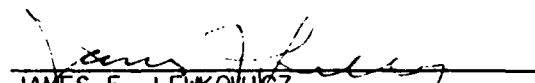
SPONSORED BY  
Defense Advanced Research Projects Agency  
Nuclear Monitoring Research Office  
ARPA ORDER NO. 5307

MONITORED BY  
Geophysics Laboratory  
Contract No. F19628-87-C-0081

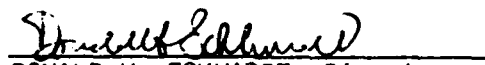
The views and conclusions contained in this document are those of the authors and should not be interpreted as representing the official policies, either expressed or implied, of the Defense Advanced Research Projects Agency or the U.S. Government.

This technical report has been reviewed and is approved for publication.

  
JAMES F. LEWKOWICZ  
Contract Manager  
Solid Earth Geophysics Branch  
Earth Sciences Division

  
JAMES F. LEWKOWICZ  
Branch Chief  
Solid Earth Geophysics Branch  
Earth Sciences Division

FOR THE COMMANDER

  
DONALD H. ECKHARDT, Director  
Earth Sciences Division

This report has been reviewed by the ESD Public Affairs Office (PA) and is releasable to the National Technical Information Service (NTIS).

Qualified requestors may obtain additional copies from the Defense Technical Information Center. All others should apply to the National Technical Information Service.

If your address has changed, or if you wish to be removed from the mailing list, or if the addressee is no longer employed by your organization, please notify AFGL/DAA, Hanscom AFB, MA 01731-5000. This will assist us in maintaining a current mailing list.

Do not return copies of this report unless contractual obligations or notices on a specific document requires that it be returned.

Unclassified

SECURITY CLASSIFICATION OF THIS PAGE

## REPORT DOCUMENTATION PAGE

1a. REPORT SECURITY CLASSIFICATION Unclassified			1b. RESTRICTIVE MARKINGS		
2a. SECURITY CLASSIFICATION AUTHORITY			3. DISTRIBUTION / AVAILABILITY OF REPORT Approved for public release; Distribution unlimited.		
2b. DECLASSIFICATION / DOWNGRADING SCHEDULE					
4. PERFORMING ORGANIZATION REPORT NUMBER(S) WCCP-R-89-01			5. MONITORING ORGANIZATION REPORT NUMBER(S) GL-TR-89-0196		
6a. NAME OF PERFORMING ORGANIZATION Woodward Clyde Consultants		6b. OFFICE SYMBOL (If applicable)		7a. NAME OF MONITORING ORGANIZATION Geophysics Laboratory	
6c. ADDRESS (City, State, and ZIP Code) 566 El Dorado Street Pasadena, CA 91101			7b. ADDRESS (City, State, and ZIP Code) Hanscom Air Force Base Massachusetts, 01731-5000		
8a. NAME OF FUNDING / SPONSORING ORGANIZATION DARPA		8b. OFFICE SYMBOL (If applicable) NMRO		9. PROCUREMENT INSTRUMENT IDENTIFICATION NUMBER F19628-87-C-0081	
8c. ADDRESS (City, State, and ZIP Code) 1400 Wilson Boulevard Arlington, VA 22209			10. SOURCE OF FUNDING NUMBERS		
			PROGRAM ELEMENT NO 62714E	PROJECT NO 7A10	TASK NO DA
			WORK UNIT ACCESSION NO. DD		
11. TITLE (Include Security Classification) Deterministic Modeling of Regional Waveforms from the Nevada Test Site					
12. PERSONAL AUTHOR(S) L. J. Burdick, C. K. Saikia and D. V. Helmberger					
13a. TYPE OF REPORT Final		13b. TIME COVERED FROM 9/5/88 TO 3/5/89		14. DATE OF REPORT (Year, Month, Day) 1989, July 19	
15. PAGE COUNT 84					
16. SUPPLEMENTARY NOTATION					
17. COSATI CODES			18. SUBJECT TERMS (Continue on reverse if necessary and identify by block number)		
FIELD	GROUP	SUB-GROUP			
			Regional Seismograms, Pn, Pn1, Synthetic Seismograms		
19. ABSTRACT (Continue on reverse if necessary and identify by block number)  (see next page)					
20. DISTRIBUTION / AVAILABILITY OF ABSTRACT <input type="checkbox"/> UNCLASSIFIED/UNLIMITED <input type="checkbox"/> SAME AS RPT <input type="checkbox"/> DTIC USERS			21. ABSTRACT SECURITY CLASSIFICATION Unclassified		
22a. NAME OF RESPONSIBLE INDIVIDUAL James F. Lewkowicz			22b. TELEPHONE (Include Area Code) (617) 377 3222		22c. OFFICE SYMBOL GL/LWH

DO FORM 1473, 84 MAR

83 APR edition may be used until exhausted  
All other editions are obsolete

SECURITY CLASSIFICATION OF THIS PAGE

Unclassified

ABSTRACT

Time domain waveform modeling studies of short period  $P_{nl}$  and high frequency  $P_n$  have been carried out in an attempt to improve event discrimination capabilities with regional data. The purpose was to develop discriminants with a well understood physical basis which could be reliably transported to different areas of the world. The study of  $P_{nl}$  involved adapting methods developed to fit long period data for observations with periods as short as two seconds. To accomplish this, we have modified the wavenumber integration method for efficient computation of  $P_{nl}$ . Long period  $P_{nl}$  is generally computed assuming a simple layer over half space model. Numerical tests were performed to determine how the model needs to be generalized to fit much shorter period data. It was found that velocity gradients like those typically observed near the free surface were of great importance. Gradients at lower depths such as at the crust-mantle transition are of much less significance. A simple layered model which accurately predicts regional  $P_{nl}$  propagation from NTS to the surrounding digital stations was developed. It deterministically explains the waveshape of the  $P_n$  and approximately the first 15 seconds of high amplitude energy reflecting past critical angle from the mantle. The modeling study of short period  $P_n$  has led to the development of an effective and physically based regional discriminant; the underlying purpose of this project. It has been found that the waveshape of the  $P_n$  is stable, similar at most stations and straightforward to model. Simple correlation of observed  $P_n$  waveforms with the expected average waveform for explosions is sufficient to discriminate events. In preceding reports, it was established that high frequency  $P_n$  appeared more to be a turning ray in the mantle rather than a classical head wave. It was also found that  $pP_n$  arrived anomalously late. In the latest work, development of  $P_n$  through its crossover was modeled, resulting in a structure appropriate for paths from NTS to Las Vegas. It was found that propagation of  $P$  to regional distances is best modeled in terms of smooth continuous positive gradients with no first order discontinuities. A model for the anomalous  $pP_n$  behavior was developed in terms of spall.



TABLE OF CONTENTS

Accession For	
NTIS CNA&I	<input checked="" type="checkbox"/>
DTIC TAB	<input type="checkbox"/>
Unannounced	<input type="checkbox"/>
Justification	
By	
Distribution/	
Availability Codes	
Dist	Avail and/or Special
A-1	

Introduction	1
Initial Work on Short Period $P_{n1}$	3
Final Results on Short Period $P_{n1}$	11
Data and Data Processing	15
Numerical Methods	22
Numerical Experiments	28
Modeling Results	39
Initial Work on $P_n$ Waveform Discriminants	46
$P_n$ Waveform Discriminants and Spall	53
Conclusions and Recommendations	64
Acknowledgements	66
References	67

## INTRODUCTION

This is the final report on a two year effort to develop effective discriminants between explosion and earthquake seismic sources which make use of regional seismic recordings. Regional body phases have proved to be among the most difficult to analyze or model in a deterministic fashion in the field of seismology. At high frequencies, the effects of scattering in the crust become so intense that only statistical properties of waveforms are meaningful. We have undertaken two investigations in this work directed at overcoming these difficulties insofar as they relate to seismic discrimination. The first was an analysis of the composition of the portion of the regional signal named  $P_n$  by Helmberger and Engen (1980). It consists of approximately the first 60 to 90 seconds of compressional signal. In the long period channel this includes the long period head wave and the PL wave which accounts for the choice of nomenclature. In the short period channel, this window would encompass high frequency  $P_n$  and  $P_g$ . The second study is an attempt to develop a discriminant based on the waveform of high frequency  $P_n$ . These two studies have several features in common. The first is that they made use of essentially the same data base; that is, records from the regional digital seismic network recently set up around the Nevada Test Site by a number of different institutions. Another is that they both take advantage of the fact that some properties of regional signals become stable and deterministic when several groups of signals are appropriately averaged together. This technique makes the best use of those properties of regional phases that are meaningful in a statistical sense. Finally, each takes advantage of an exception to the generality that regional phases are too unstable to model with synthetic seismograms. This is apparently not true at longer period or at very short times at the beginning of the signal.

Three interim reports have been distributed chronicling the progress of these investigations. We begin with a brief summary of previous work on short period  $P_{n1}$  which is relevant to the final outcome of the investigation. We then discuss the final results on this portion of the study. We present a similar synopsis of previous work and finally results on studies of short period  $P_n$  waveforms.

### INITIAL WORK ON SHORT PERIOD $P_n$

The initial motivation for investigating the physical nature of the short period energy in  $P_n$  came from the recognition that it would be very useful to develop ways to passively calibrate regional arrays. When regional networks are installed in new areas for monitoring purposes, it can be anticipated that they will be of limited use because of uncertainties about regional wave propagation in the place where they are located. However, they will immediately begin to record small to moderate sized earthquakes at regional distances. Events in the magnitude range of 3 to 5 occur regularly in every continental area and most of these events will be reliably identified as either explosions or earthquakes by standard methods. Figure 1 shows a typical broad band regional signal from an earthquake recorded at a modern digital station. These are the compressional signals from the Idaho earthquake of October 29, 1983 as recorded at RSSD. Even though the magnitude was only 5.4, the event produced a clear signal 800 km away on all three channels. The long period trace is very simple and can be easily modeled using standard long period methods. The intermediate trace is much richer in character. The  $P_n$  onset is weak followed by two stronger arrivals which are the depth phases  $pP_n$  and  $sP_n$ . There is a distinct large amplitude arrival about twenty seconds into the record with a simple enough character to warrant an attempt at deterministic modeling. An examination of the particle motion shows that some scattering by non stratified structure is occurring. The bottom short period channel exhibits a typical high frequency regional P wave. There is a high frequency  $P_n$  followed by  $P_g$ . The relationship between  $P_g$  onset and the phase on the intermediate channel is intriguing. The particle motion in the short period channel indicates strong scattering with equal energy appearing on the tangential, radial and vertical traces. The clear implication of Figure 1 is that there is a breakdown of deterministic character of the signal



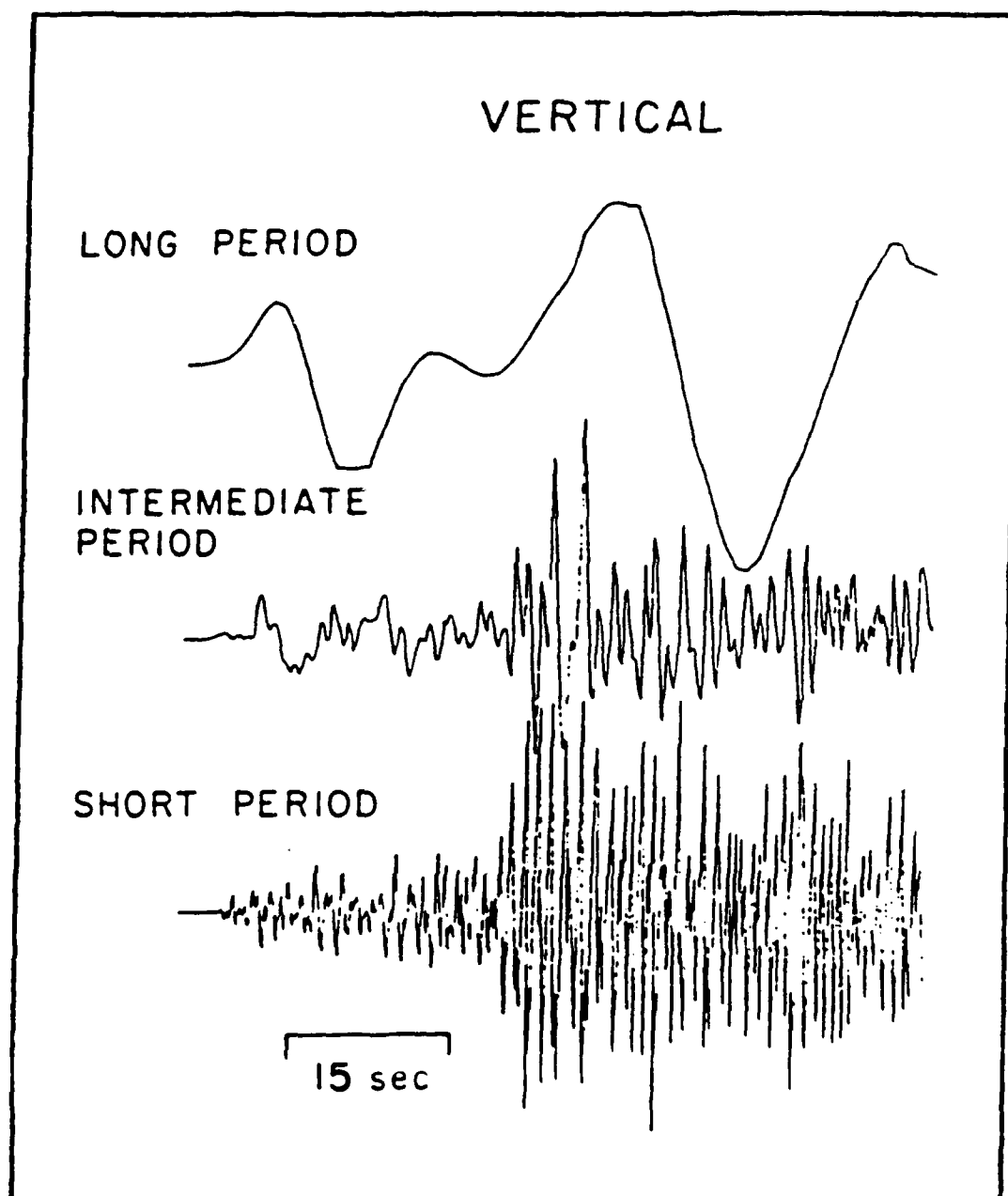


Figure 1. Long, intermediate and short-period vertical Channels,  $P$  waves from the Idaho earthquake of October 29, 1983 ( $M=5.4$ ) as recorded at RSSD ( $R=800$  Km). Seismograms are displayed on the same time scale. First arrival is  $P_n$ . The onset of large amplitude waves is the arrival time of  $P_g$ .

descending down the page. However, it would appear that if the top two traces could be deterministically modeled, they would serve as a useful guide to interpretation of the short period signal.

The basis of what we suggested in our first report (Burdick and Helmberger, 1987) was that if broad band signals recorded at newly installed regional stations were routinely modeled, a predictive capability could be developed for given paths. Synthetic long and intermediate period seismograms could be computed for any path from which a reference event was available. The utility of these synthetics is that they help to identify when phases high in discrimination potential such as depth phases or shear phases arrive. Unidentified seismic events are generally small and recorded only on the short period channel. Longer period synthetics could be computed for them using the calibration models developed over time and discrimination capability could be increased.

We discussed our forward modeling efforts on the data in Figure 1 in our first report. Some of the results are shown in Figure 2. The short period synthetics shown were computed using the formalism outlined in Helmberger and Engen (1980) along with their layer over a half space model and the correct intermediate period instrument response. The synthetics show a series of resonating high amplitude arrivals which are also present to some extent in the data. We named these phases crustal resonance phases and examined their composition in terms of generalized rays. As might have been suspected, these resonances are associated with successively higher orders of reverberations in the crust. Interestingly, the second resonance phase is not associated with the second order of reverberation, but with rays that have at least one converted S leg. Thus, a comparison of the first to the second resonance might have discrimination potential. To compute complete  $P_{n1}$  synthetics, Helmberger and Engen (1980) typically included 4094 generalized rays in the ray set. By examining small

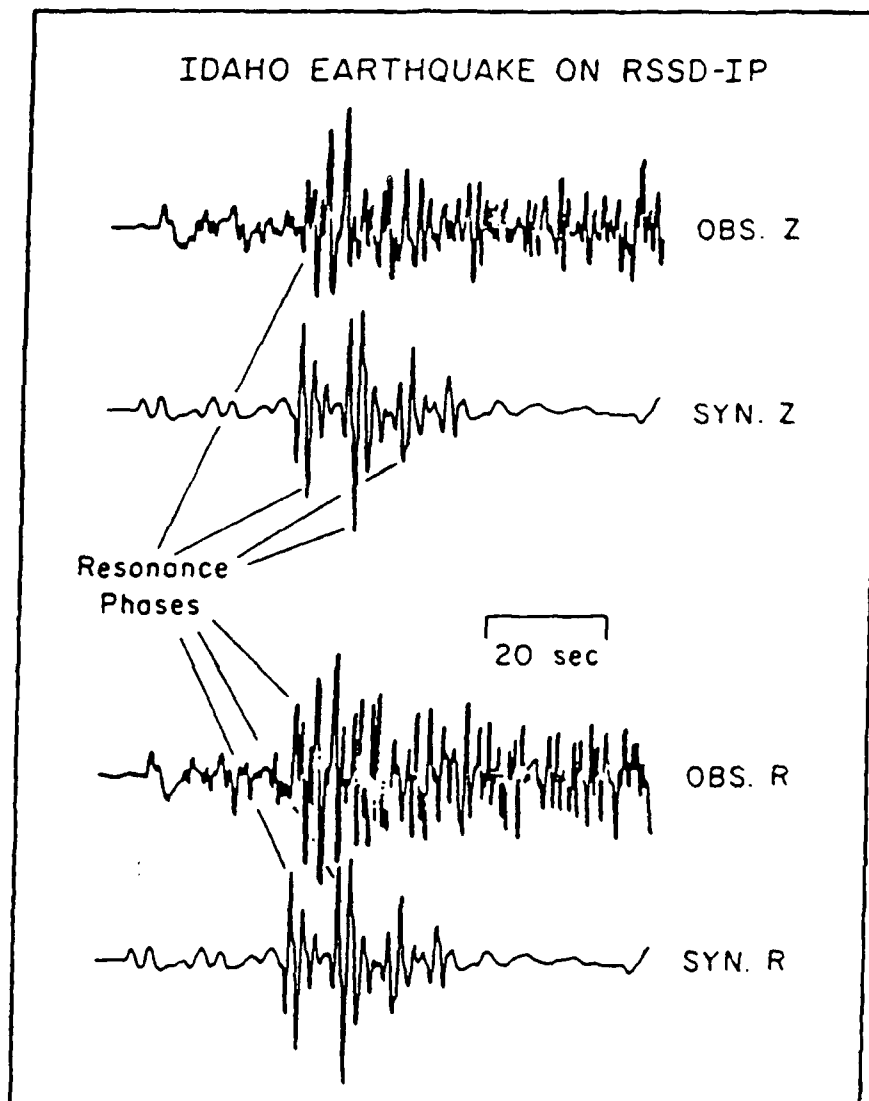


Figure 2. A comparison between observed and synthetic intermediate period *P* wave seismograms for both vertical and radial components from the Idaho earthquake of October 29, 1983 (M-5.4). Crustal resonance phases are identified. The synthetics were computed using the methodology of Helmberger and Engen (1980).

subsets of rays, we established that the first resonance phase is dominated by the six rays P, S, PmP, pPmP, SmS and sSmS. The S rays contribute through the phenomenon of S to P diffraction. The second resonance is controlled by the eight rays PmS, SmP, pSmS, sPmP, PmPSmS, SmSPmP, PmPSmP and PmSPmP. We performed additional studies which indicated that the  $P_n$  signals behave more like turning rays than true head waves, but this is more relevant to the second of our investigations as discussed below.

To further establish the existence and stability of resonance phases at even higher frequencies, we attempted stacking high frequency signals from NTS explosions as observed at the DWSSN station ALQ. The results were discussed in our second report (Burdick et al., 1988). An example of the results is shown in Figure 3. The crustal resonances emerge clearly as the traces are progressively summed. A synthetic for the layer over a half space model is shown at the bottom. Again the correspondence between data and synthetics suggests that the composition of Pg in terms of its energy is much like that in the simple crustal model. This, however, raises many interesting questions. The crust in the western U.S. is certainly not a simple layer over a half space. It contains strong gradients, at least at the surface and strong lateral variations in thickness. This should cause large discrepancies between data and synthetics at least at short periods. We report our investigations into these questions next.

Finally, we presented in our second report some preliminary results indicating that crustal resonance phases might be useful for event discrimination. It appears that the first resonance phase is primarily a channel for compressional energy. The second is a much more efficient channel for converted energy. At short periods in the real earth, energy traveling in these channels will be highly scattered, but there should be more shear energy in the second channel. Thus, the second channel may be more strongly excited by sources richer in shear

PROGRESSIVE SUM OF RECORDS  
YUCCA TO ALQ OR ANMO

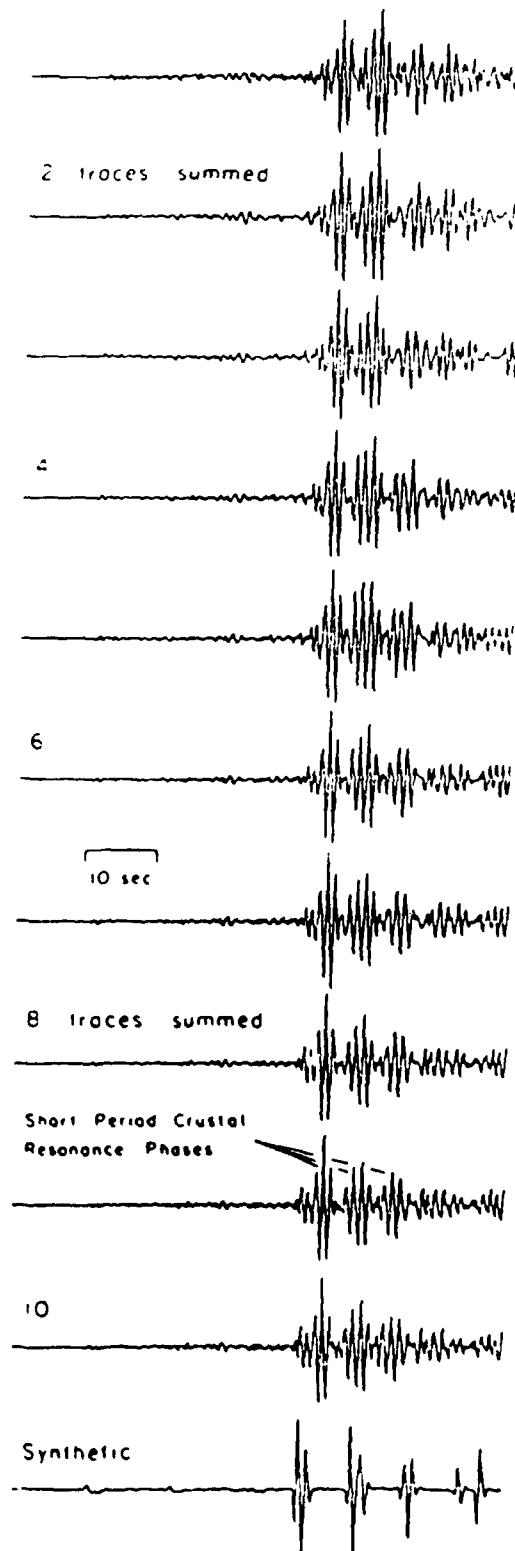


Figure 3. Enhancement of crustal resonance phases for Yucca explosions recorded at ALQ or ANMO by progressive sum of seismograms. The synthetic at the bottom merely indicates that the phases have approximately the right timing and amplitude.

energy. Figure 4 compares averaged three component records for Pahute explosions observed at ANMO to vertical and radial synthetics for the simple crustal model. It is clear that the particle motion changes in the synthetics between the first and second crustal resonance phase. Because of interference effects the second resonance phase is suppressed on the radial. The same happens in the stacked observations. The tangential record suggests that there are bursts of scattered energy perhaps associated with the crustal resonance channels.

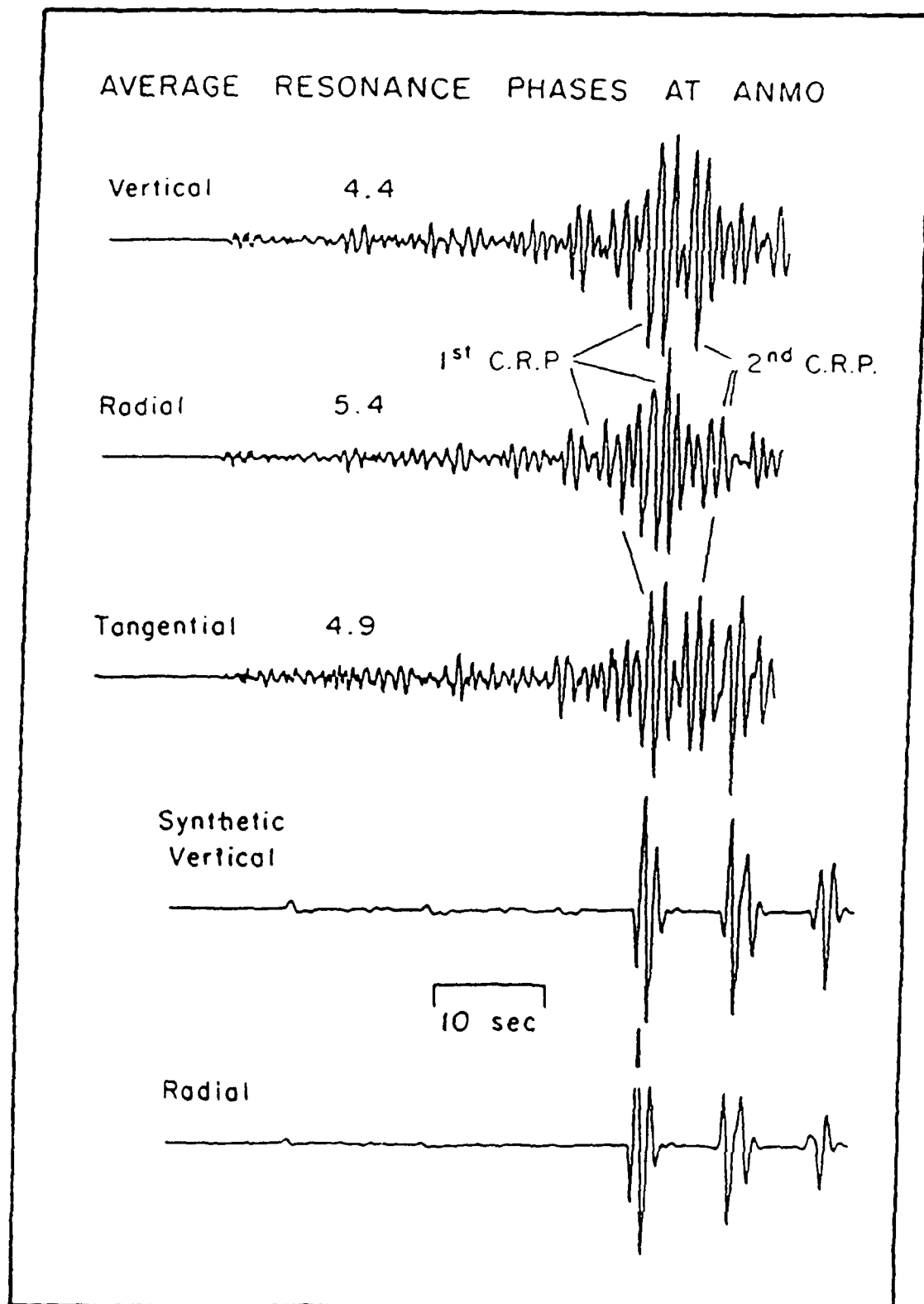


Figure 4. Average three-component seismograms recorded at ANMO and obtained by stacking the explosions from Pahute Mesa. Evolution of the particle motion between the first and second crustal resonance phases is clear. Synthetics were computed to predict the observed particle-motion evolution.

### FINAL RESULTS ON SHORT PERIOD $P_{n1}$

Long period  $P_{n1}$  from explosions and earthquakes has been modeled previously in a number of significant and remarkably successful investigations. In the first of these, Helmberger (1972,1973) modeled the long period P waveforms from NTS explosions as they progressed from waves trapped in the crust into diffracted waves in the shadow zone and finally into waves turning in the upper mantle. This work resulted in a widely accepted model for the velocity and Q structure of the low velocity zone. The next investigation was the one discussed above by Helmberger and Engen (1980) who focused on the waves trapped in the crustal wave guide. They detailed procedures for computing synthetics and introduced the term  $P_{n1}$  waves to describe the composite of long period  $P_n$  and PL energy. In subsequent investigations, Wallace et al. (1981) and Wallace (1986) demonstrated that long period  $P_{n1}$  waveforms are stable and deterministic enough to be utilized in automated inversion schemes for source mechanisms or crustal structure. The investigations of Somerville (1986), Lefevre and Helmberger (1989) and Holt and Wallace (1989) demonstrated that the  $P_{n1}$  analysis procedures could be applied without substantial modification to observations from virtually any tectonic regime. Figure 5 shows the locations and mechanisms of the events in the North American continent for which  $P_{n1}$  waves have been successfully modeled. The applicability of the technique clearly does not depend on fault mechanism or on tectonic environment. In this investigation, we have returned once more to observations of  $P_{n1}$  from NTS explosions as in the first studies. However, we extend the analysis down to much shorter periods. The earlier investigations all focused on energy with periods longer than about 10 seconds. We here discuss the analysis of data with periods as short as 2 seconds.



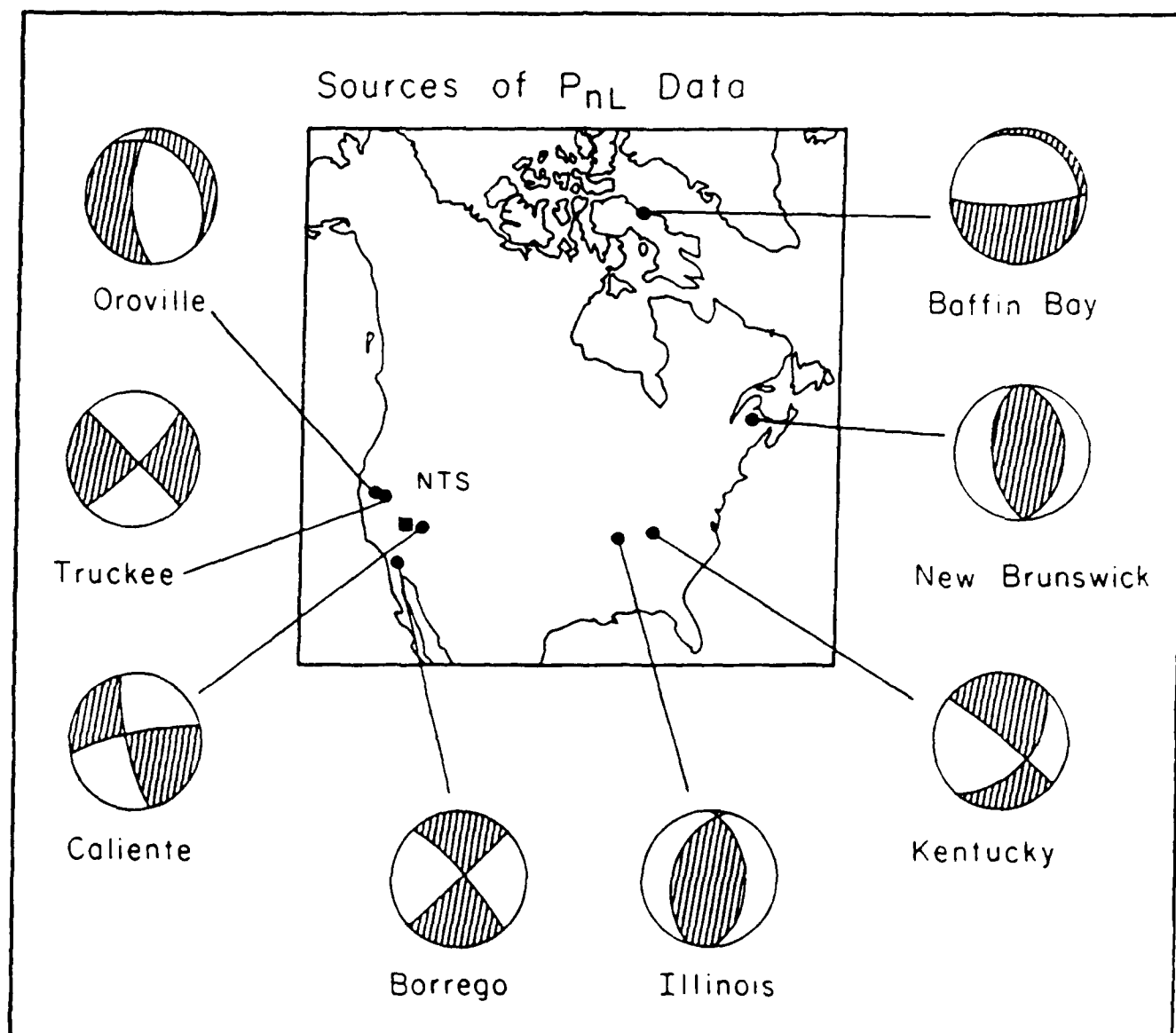


Figure 5. Location and focal mechanism of individual earthquakes of the North American continent for which the long-period  $P_{nL}$  seismograms were successfully modeled.

Additional motivation for attempting such a study is illustrated in Figure 6. There we compare observed to synthetic  $P_{n1}$  waves for the 8/16/66 Caliente earthquake and the 1/9/82 New Brunswick earthquake. Their locations are shown in Figure 5. The correspondence of the long period character in the data and synthetics is very apparent. It is a remarkable fact that exactly the same crustal structure was used in calculation of the synthetics for these two events. It was the simple one layer over a half space model introduced in the Helmberger and Engen (1980) paper. In fact, this same simple model has been used in most of the above mentioned studies to model  $P_{n1}$  all over the world. The success of the model in predicting the observations in the various tectonic regimes is somewhat surprising since it is widely recognized that the crust in the Canadian shield is almost twice as thick as in the western U. S. and significantly higher in velocity. The general success of this simple model is explained, however, by the fact that at long period the earth does behave like a layer over a half space. The detailed nature of the crust is not significant. In Figure 6, we have connected with short line segments some of the shorter period details in the data and synthetics which appear to correspond. This shorter period energy will certainly be very sensitive to details of crustal structure in the two tectonic regions. Yet the features connected by the line segments appear as if they would match with only moderate adjustments of the crustal structure.

There have been significant advances in the last few years both in the field of seismic data recording and in computational seismology. Data is now recorded digitally and advanced computers permit rapid calculation of relatively exact synthetic seismograms in many layered structures. In this study, we have taken advantage of these developments to try to model some of the finer details of the  $P_{n1}$  signals from NTS explosions.

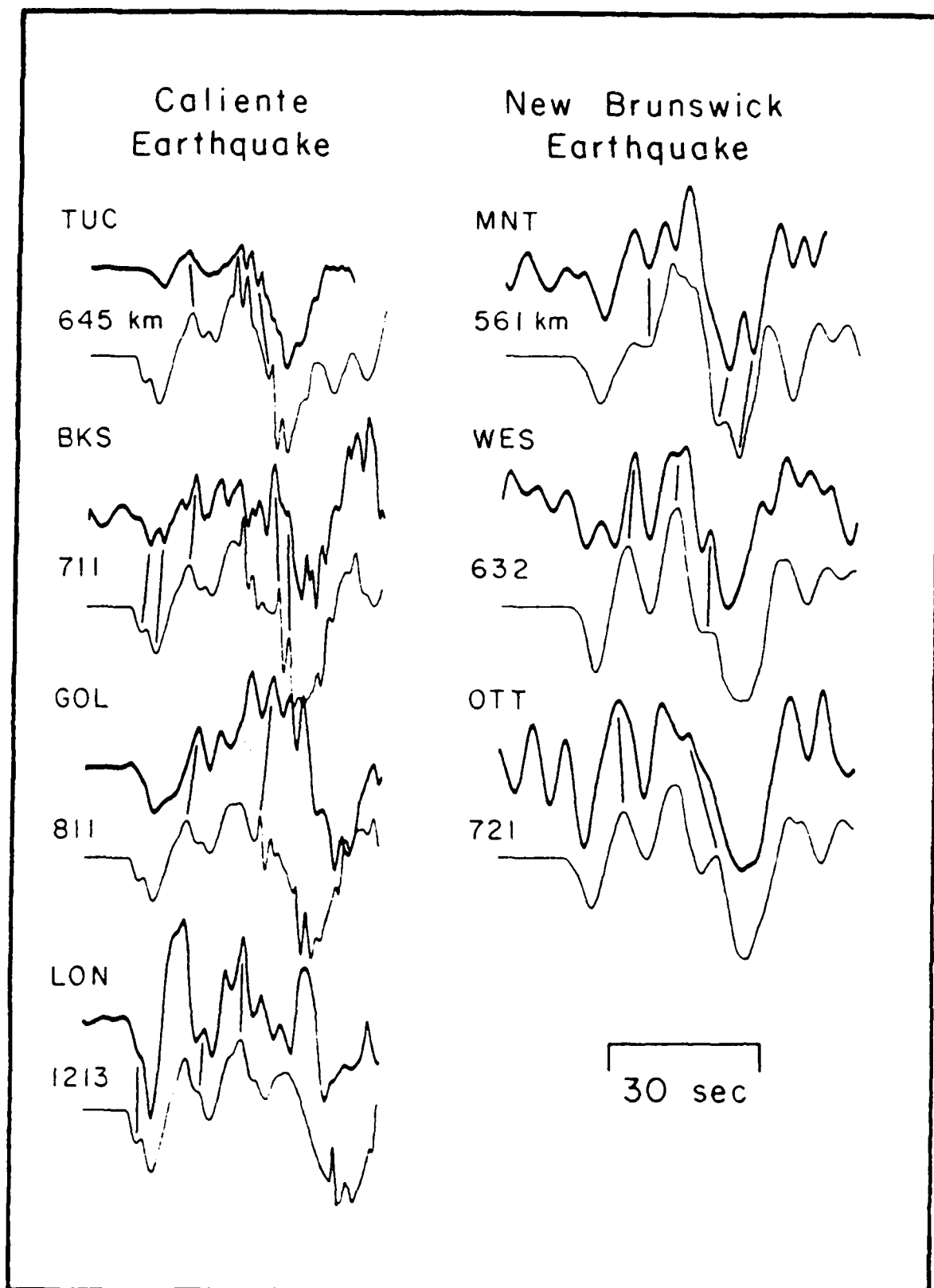


Figure 6. *P<sub>n</sub>L* seismograms from earthquake sources showing the correlation between data (dark lines) and synthetics. Near vertical lines show the features that are well correlated.

DATA AND DATA PROCESSING Modern broad band digital recording systems are rapidly becoming commonplace throughout the world, particularly near such important data sources as the Nevada Test Site. Unfortunately, methods of cataloguing and distributing data remain diverse in nature and efficiency. Figure 7 shows the eight regional stations around NTS from which we assembled the data base for this investigation. The two stations ALQ and JAS are part of the DWSSN, the four stations MNV, ELK, KNB and LAC are Lawrence Livermore National Laboratory stations and PAS and PFO are operated independently by universities. The data from the DWSSN is the most generally accessible from the network.  $P_{nl}$  signals from approximately 30 events for each of the two stations were plotted and reviewed for possible use. Data from the LLNL network is not routinely made generally available. However, representative data bases are occasionally released. A suite of 24 events were reviewed for possible use. The new broad band digital stations at Pinyon Flat and Pasadena were installed most recently. The instruments are new state-of-the-art Streckeisens, but they have only been in operation for a brief time. Seismic data from 6 nuclear tests were provided by the observatory for possible use in the study. The data from Pasadena station may be accessed through a telephone link, but only a brief historical backlog exists. Signals from eight recent tests were collected and reviewed.

The instruments at the eight stations vary in their characteristics. The DWSSN signals are comparatively band limited with respect to all of the others. The other six stations record broad band high dynamic range signals. To standardize our data base, we corrected all signals to the effective WSSN response. This response was selected because accurate broad band information is difficult to recover from the DWSSN data, and WSSN records have been used in virtually all of the previous  $P_{nl}$  studies. Initial review of the data indicated that there was a great deal of stability in the  $P_n$  signals from the large events and also

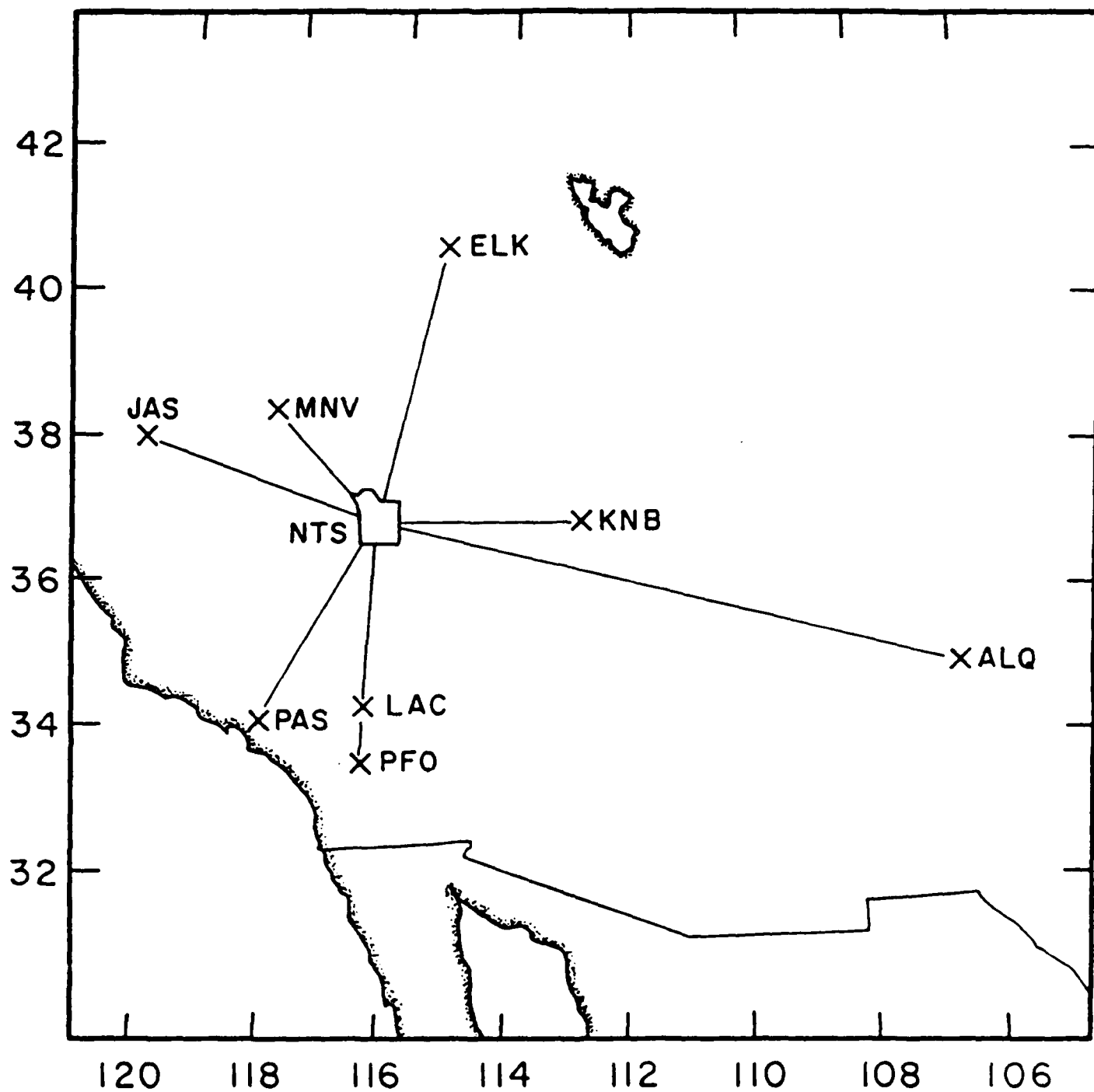


Figure 7. Map showing the distribution of stations from NTS. Of these ELK, KNB, LAC and MNV are broad band stations operated by LLNL; the stations ALQ and JAS are operated by DWWSSN and the stations PAS and PFO by universities.

consistency in the PL especially near the PL onset. At later times in the record, the effects of scattering begin to dominate and the signals at any given station become highly variable from event to event. Accordingly, sections of the signals from all of the events being reviewed were windowed out including a 10 second leader, all of the  $P_n$  train and about 15 seconds at the front of PL. We will discuss the composition of this last part of the signal in much more detail in the following. We will show there that, depending on choice of nomenclature, this last part could as correctly be described as the onset of the regional phase  $P_g$  or the 15 seconds after the arrival of the Moho reflection  $PmP$ .

The original instrument response for each signal was deconvolved out and the WWSSN response convolved in. A further bandpass filter was applied to the signals. The form of the filter for both high and low pass was a standard third order Butterworth given in the Laplace domain by

$$F(s) = \frac{\omega_l}{s + \omega_l} \frac{\omega_l^2}{s^2 + \cos(\pi/6)\omega_l s + \omega_l^2} \quad (1)$$

where  $s = i\omega$ . The above filter was designed in the Z-domain using the bilinear Z-transform and filtering was performed in the time domain. The low pass value for  $\omega_l$ , the cutoff frequency, was set at 0.6 hz. As discussed in the next section, this made computation of synthetics using a wave number integration approach relatively practical. The same Z-domain functional form of a low pass filter becomes a high pass filter if  $s$  is replaced by its inverse and the cut-off frequency  $\omega_h$  is defined as  $1/2\Delta t - \omega_h$ . The high pass cutoff was set at 0.1 hz to eliminate long period offsets and drifts.

Because of extant yield threshold agreements, all events detonated at NTS since installation of the digital network have been relatively small ( $m_b < 6$ ). It is well known that microseismic noise is a significant source of signal contamination for events of this size at the distances and period range under

consideration. In reviewing the data base, we found that the  $P_n$  wavetrain in particular was below the noise level in very many cases. We were able to find within the data base, however, several signals for large events on quiet days in which  $P_n$  signal to noise ratios were good. Comparisons of these signals demonstrated that the waveshapes were consistent through the  $P_n$  and the onset of high amplitude reflected energy. Though the uncertainties associated with background noise were substantial, it was found that the entire data base indicated that deterministic modeling of this part of the wavetrain would be meaningful. Figure 8a illustrates this stability for 3 different events at each of the 4 LLNL stations for Yucca Flat events. The move out of  $P_n$  in front of the strong reflected energy as distance increases is apparent. The consistency of the short period details in the waveforms is even more striking than in the earthquake data in Figure 6. A similar comparison of signals for Pahute Mesa events is presented in Figure 8b. The strong correlation of the signals is again apparent. There are differences between the Yucca Flat and Pahute Mesa signals at the same station, but this is not surprising given the variation in distance to the sites.

Figure 9a compares the waveforms for 3 of the remaining stations in the digital net for Yucca Flat events. Because of the very limited number of events available from PAS, we were only able to find two events with acceptable signal to noise. No suitable two Yucca Flat events at all were in the 6 signals available from PFO. Nonetheless, our basic observation regarding the stability of the beginning of the wave train holds true. The observations from ALQ are particularly remarkable given that the station is so far away. The  $P_n$  wave train is almost 30 seconds long, but the strong reflected energy remains very stable. A deterministic modeling study would clearly be appropriate. Figure 9b presents

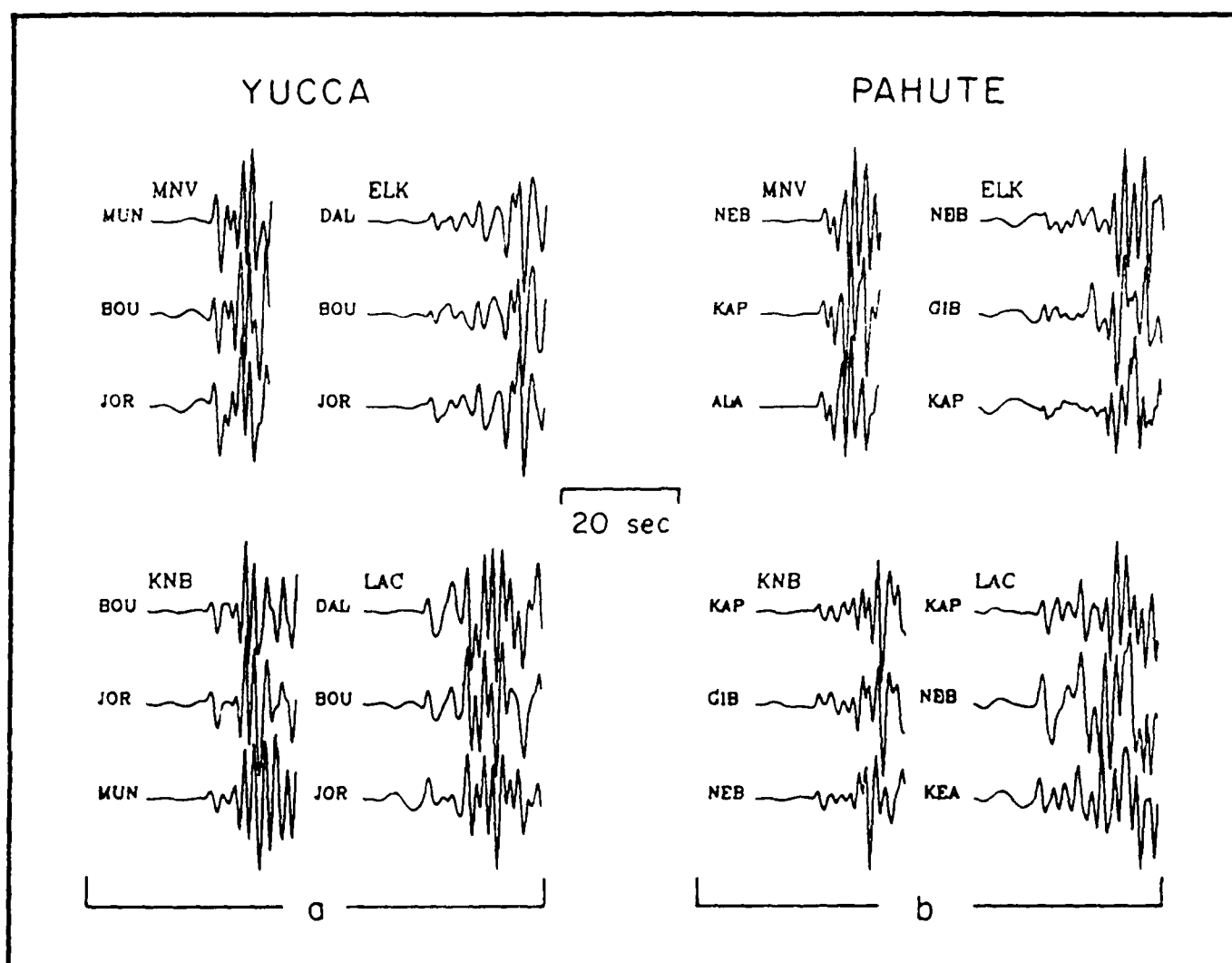


Figure 8. Recorded  $P_{n1}$  seismograms from both Yucca flat and Pahute Mesa on the LLNL network after convolving with a WWSSN LP instrument and a recursive bandpass filter (low-cut = 0.1 Hz, high cut = 0.6 Hz and third-order Butterworth causal). (a) For Yucca flat explosions and (b) for Pahute Mesa explosions. Data show remarkable stability. Original instrument response was deconvolved.



## YUCCA EVENTS

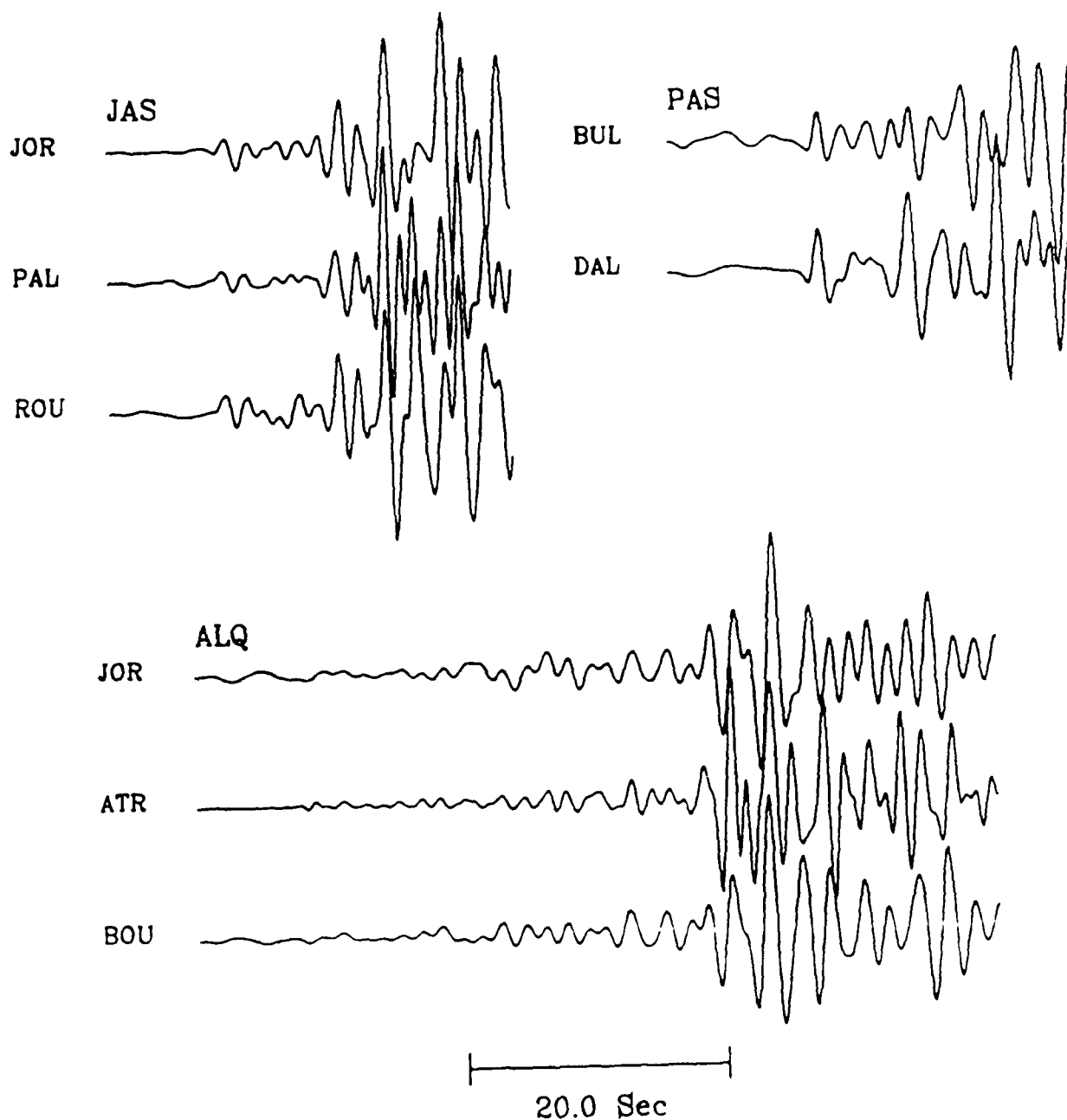


Figure 9a. Recorded  $P_{nl}$  seismograms from Yucca flat explosions at JAS, PAS and ALQ after convolving with a WWSSN LP instrument and a bandpass filter (low-cut = 0.1 Hz, high cut = 0.6 Hz and third-order Butterworth causal). Original instrument response was deconvolved. The data show remarkable stability.

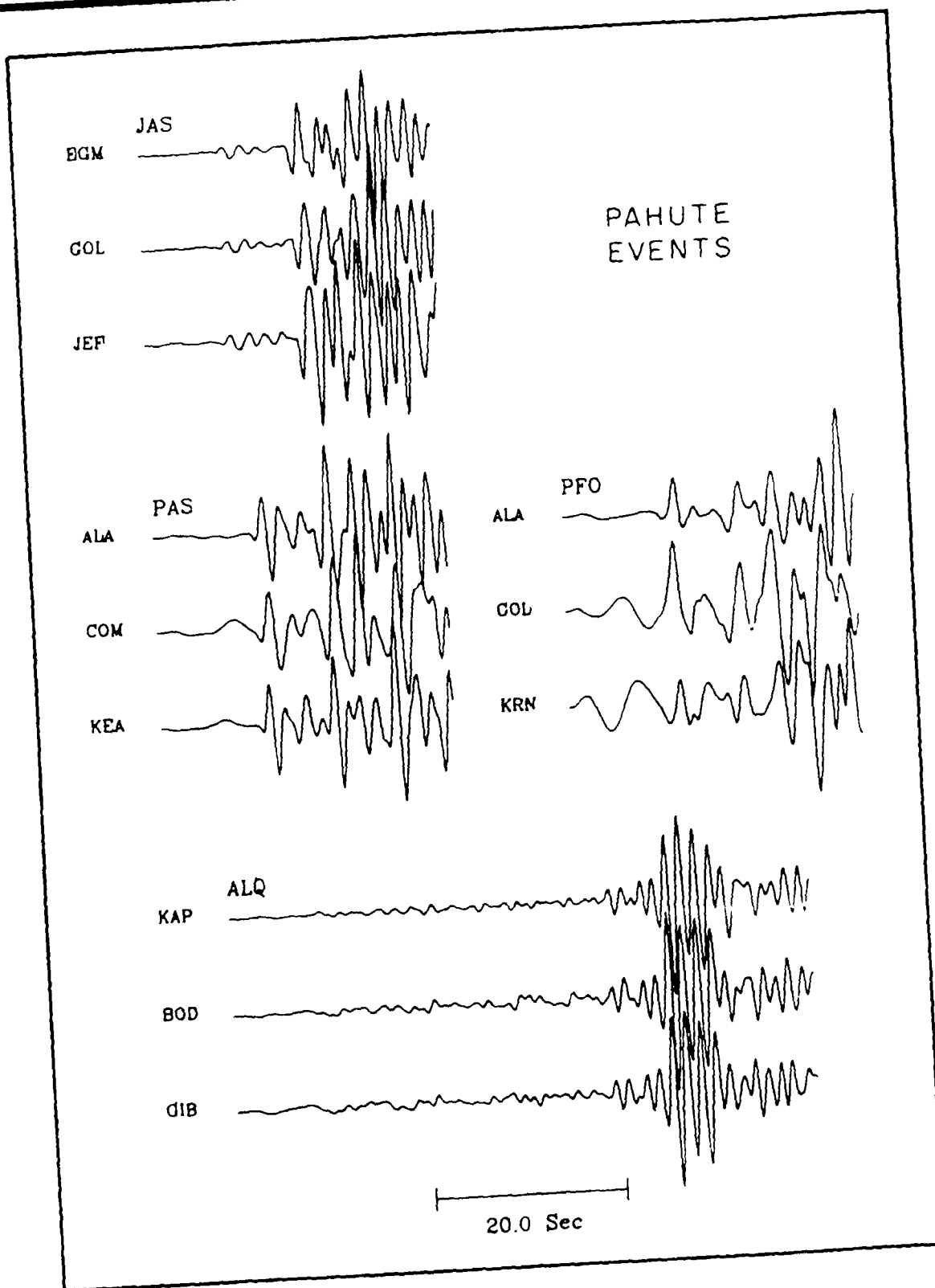


Figure 9b. Recorded  $P_n$  seismograms from Pahute Mesa explosions at JAS, PAS, PFO and ALQ after convolving with a WWSSN LP instrument and a bandpass filter (low-cut = 0.1 Hz, high cut = 0.6 Hz and third-order Butterworth causal). Original instrument response was deconvolved. The data show remarkable stability.

a similar comparison for Pahute Mesa events for the remaining 4 stations in the digital net including PFO this time. Modeling these waveforms has been the primary goal of this study.

Numerical Methods  $P_{nl}$  waveforms can be synthesized at regional distances by a variety of techniques. The two most practical are generalized rays and full-wave synthesis. The generalized ray approach is the most efficient for a layer over a half space model and has been used in most previous  $P_{nl}$  studies. It becomes difficult to obtain exact results in a multilayered model because the ray sum becomes intractably large. One real utility of the method is that it allows decomposition of the wave field into individual rays. We will take advantage of this facet to some extent in the following. The full-wave synthesis approach can be effectively used to produce an accurate estimate of the wave field in a finite frequency band for a complex layered model. However, some steps must be taken to band limit both the wavenumber and frequency integrals to keep the method truly practical. Alternate approaches to computing the synthetic seismograms are the frequency-wavenumber ( $f-k$ ) scheme (Wang and Herrmann, 1980; Bouchon, 1981) and the reflectivity approach (Kennett, 1980; Mallick and Frazer, 1987). Our primary numerical tool in this work has been a modified version of the Wang and Herrmann (1980) method.

We developed a vectorized computer program based on the formulation presented by Wang and Herrmann (1980). For a medium consisting of  $n$  laterally homogeneous layers and a source embedded at an interface  $m$  the  $f-k$  kernels are evaluated using the expression

$$\begin{pmatrix} U_r \\ U_s \end{pmatrix} = -\frac{1}{R_{12}^{12}} \begin{pmatrix} \zeta_r X_{12}^{12} Z_{12} \\ -\zeta_r X_{12}^{12} Z_{11} \end{pmatrix} \quad (2)$$

where

$$X|_{ij}^{12} = (FE_N^{-1})|_{mn}^{12} \alpha_{n-1}|_{pq}^{na} \dots \alpha_{m+1}(d_{m+1})|_{ij}^{n'}$$

$$R|_{12}^{12} = (FE_N^{-1})|_{mn}^{12} \alpha_{n-1}|_{pq}^{na} \dots \alpha_1|_{12}^{n'}$$

$$\alpha|_{ki}^{n'} = \alpha_{ik}\alpha_{ji} - \alpha_{it}\alpha_{jk} \quad (3)$$

$$Z = \alpha_m \alpha_{m-1} \dots \alpha_1$$

(the  $\alpha_{ij}$ 's being the elements of the original Haskell's (1964) matrix). The explicit forms of  $FE_N^{-1}$ ,  $\alpha|_{ki}^{n'}$  and  $\zeta_i$  (the source coefficients) are given in Wang and Herrmann (1980). Expression (2) together with the expressions (3) allow the propagation of the stress-displacement vector from a half-space through a layered medium with a source discontinuity to the free surface. It involves propagation of the stress-displacement vector with the use of compound matrices  $R|_{12}^{12}$  and  $X|_{ij}^{12}$  (Dunkin, 1965; Watson, 1970). These compound matrices are the product of matrices of subdeterminants. They have an advantage over the Haskell matrices in that the square of the exponential terms have been canceled out in the analytical formulation of  $\alpha|_{ki}^{n'}$  matrix. This eliminates the loss of significant figures in the multiplication and subtraction of the original Haskell matrix elements (Dunkin, 1965).

The  $f$ - $k$  kernels  $U(r, k, \omega)$  are integrated to obtain the medium response  $U'(r, \omega)$  using the Fourier-Bessel transformation

$$U(r, \omega) = \int_0^\infty U(r, k, \omega) k J_0(kr) dk \quad (4)$$

For the evaluation of the regional wavefield, we have approximated the Bessel functions by the principal asymptotic form of the Hankel function representation of the out-going wavefield. With these approximations, the final expression used to integrate the kernels is

$$U(r, \omega) = \sqrt{\frac{2}{\pi r}} \int_0^\infty \sqrt{k} U(r, k, \omega) e^{-i(kr - \pi/2 - \pi/4)} dk \quad (5)$$

We use  $F(\omega) = \int_{-\infty}^{\infty} f(t) e^{-i\omega t} dt$  for FFT. Wavenumber integrals are evaluated using equal

sampling in  $k$  domain (Bouchon, 1981) and inversion to the time domain using an FFT algorithm. The code and the reflectivity code developed by Mallick and Frazer (1988), based on Kennett (1980), were calibrated against each other. The results agreed very closely, and the  $f$ - $k$  algorithm proved to be more economical for computing the free surface displacement in the frequency band of our interest.

The time window of interest in  $P_{n1}$  studies is approximately one minute after the first arrival. At regional ranges, the entire signal is dispersed considerably lasting for up to 10 minutes. Since the spectrum of the complete signal is automatically computed by the method, this later energy can strongly affect the spectrum in the time window of interest through the phenomenon of wrap around if a short time window is chosen. Several possible approaches for overcoming this problem have been suggested in the literature, and we have investigated three of them. These include integration on a displaced contour in the frequency domain (Phinney, 1965; Bouchon and Aki, 1977; Spudich and Ascher, 1983), wavenumber filtering and computation of an extended time series to damp out wrap around, and we have tested all three. We have also investigated the importance of  $Q$ .

The damping technique of Phinney (1965) involves giving frequency a small, constant imaginary part  $\alpha$  which has a two-fold purpose. One is the shifting of the poles of the  $f$ - $k$  kernels from the real  $k$  axis into the fourth quadrant of the complex  $k$  plane. Consequently, integration can be performed along the real  $k$  axis without any problem. The use of complex frequency also has the effect of multiplying the true response  $f(t)$  by a factor of  $e^{-\alpha t}$ . Mallick and Frazer

(1987) showed via an elegant Fourier transform pair that the evaluation of response  $f(t)$  using the complex frequency technique produces a time domain response equivalent to

$$e^{-\alpha t} \left[ f(t) + \sum_{n \neq 0} f(t+nT) e^{-\alpha nT} \right] \quad n = \dots, -2, -1, 1, 2, \dots \quad (6)$$

i.e. it suppresses the response  $f(t+nT)$  outside the time window  $T$  by a factor  $e^{-\alpha(t+nT)}$ . They suggest a rule of thumb in selecting  $\alpha$  of  $1/D = e^{-\alpha T}$  where the maximum allowable value of  $D$  is 50 and  $T$  is the total length of the time series. This damping is then corrected for in the final time domain synthetics. Bouchon (1979) suggested that  $\alpha$  should be chosen such that  $e^{-\alpha T} \ll 1$ . Herrmann (1985) pointed out that  $\alpha T = 2$  is a reasonable choice. He also suggested that some trial and error testing may be necessary to set this parameter. As we show in the following, our experiments with a simple crustal model indicate that a higher value of  $D$  will cause spurious noise which originates due to the values of  $\omega$  which no longer satisfy the condition  $\omega \gg \alpha$ .

Our test model was simply a layer over a half space with a few low velocity layers on top to represent the surface gradient. Our initial selection for time series length was 1024 points with a Nyquist frequency of 5 hz.  $D$  was set at 50. The source is a shallow explosion and the range is 300 km. Here and throughout we utilize the Murphy (1971) wet tuff source time history. The results are shown in the top row of Figure 10. The notation above the trace indicates the value of  $\alpha$ , that no  $Q$  correction is applied and no wave number filter is used. The notation is self explanatory for the rest of the traces. Though the synthetic looks generally reasonable the contamination of the  $P_{n1}$  is severe. The short trace on the right is an amplification of the  $P_{n1}$  from the left trace, and it clearly shows high amplitude acausal energy at the beginning. We next attempted increasing the number of points to 4096. We reduced the Nyquist to 2.5 in an

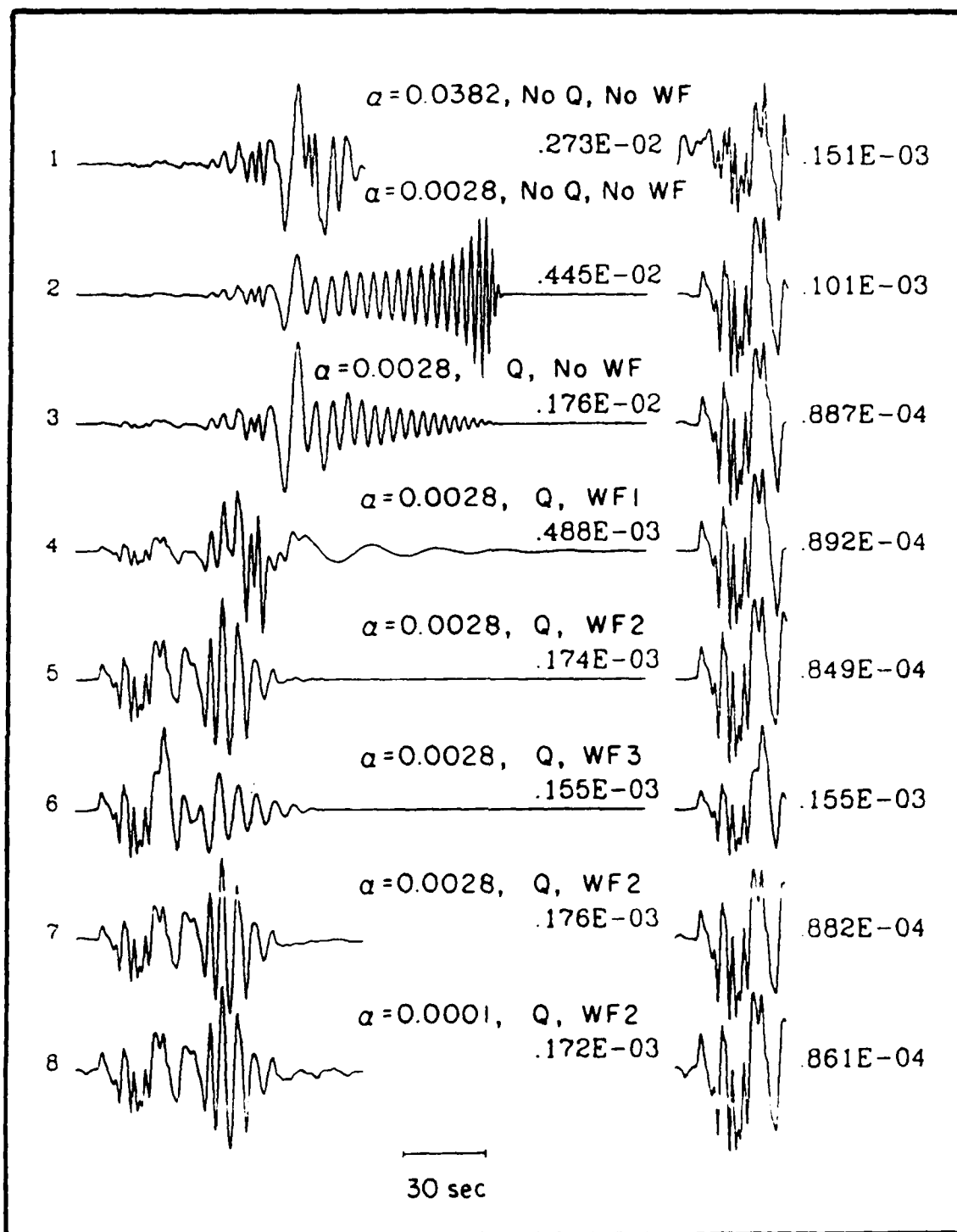


Figure 10. A suite of theoretical WWSSN long-period seismograms computed using a vectorized  $f-k$  algorithm from a half-space model with a gradient-like structure in the upper six kilometers. Seismograms on left demonstrate the effects of various  $Q$ , ray-parameter filters, complex frequencies and length of time series. On right are plotted the  $P_{nl}$  seismograms of this study.

effort to improve efficiency and reduced D to 10 to improve accuracy. The required increase in computation time for the longer time series was still very large. The traces in the second row in Figure 10 show the result. The complete signal on the left shows unrealistically high amplitude higher mode surface waves. In the real earth this type of energy would ordinarily be attenuated or scattered out. Anelasticity was introduced through complex compressional and shear wave velocities ( $\alpha_i, \beta_i$ ) complex as given by

$$\begin{aligned}\alpha_i(\omega) &= \alpha_i \left[ 1 + \frac{1}{\pi Q_{\alpha i}} \ln \left( \frac{\omega}{\omega_r} \right) - \frac{i}{2Q_{\alpha i}} \right] \\ \beta_i(\omega) &= \beta_i \left[ 1 + \frac{1}{\pi Q_{\beta i}} \ln \left( \frac{\omega}{\omega_r} \right) - \frac{i}{2Q_{\beta i}} \right]\end{aligned}\quad (7)$$

where  $\omega_r$  is reference frequency (Aki and Richards, 1980). We chose this reference frequency to be 1 Hz. A relationship of  $Q_\alpha = 2Q_\beta$  was used for  $Q_\alpha$ . The near-surface  $Q_\beta$  structure was taken from the basin and range province of the Western United States (Wen, 1989). The realistic looking results are shown in the third row. The  $P_{n1}$  portions of the seismogram on the right of rows two and three can be considered as the "correct" synthetics. Our additional efforts were directed at finding a way to compute them efficiently. A comparison between the  $P_{n1}$  waves in rows 2 and 3 indicates that attenuation has little effect on the waveshape and a small effect on amplitude. Thus, it is not important to know the Q structure accurately to compute  $P_{n1}$  in this frequency band. We next considered the possibility of wave number filtering and used the same Q structure.

The filter we applied was a simple cosine taper defined in ray parameter domain by

$$F(p) = \begin{cases} \frac{1}{2} \left[ 1 - \cos \left[ \frac{\pi(p - p_{min})}{p_1 - p_{min}} \right] \right] & p_{min} \leq p \leq p_1 \\ 1.0 & p_1 \leq p \leq p_2 \\ \frac{1}{2} \left[ 1 + \cos \left[ \frac{\pi(p - p_2)}{p_{max} - p_2} \right] \right] & p_2 \leq p \leq p_{max} \end{cases}\quad (8)$$



The values of  $p_{\min}$  and  $p_1$  were fixed at 0.0001 and 0.033 sec km<sup>-1</sup>, and the effects of the high  $p$  cutoff were tested. Figure 10 shows the results of  $p_2=0.285$  and  $p_{\max}=0.288$  sec km<sup>-1</sup> (WF1),  $p_2=0.222$  and  $p_{\max}=0.244$  sec km<sup>-1</sup> (WF2) and  $p_2=0.200$  and  $p_{\max}=0.220$  sec km<sup>-1</sup> (WF3). The goal is to select parameters which preserve both the shape and amplitude of the  $P_{n1}$  waveform. As indicated in the figure, WF1 leaves too much long period and WF3 distorts the waveform substantially. The parameters of WF2 give acceptable results. We examined the possibility of abandoning the complex frequency damping in light of the efficiency of the wavenumber filter in reducing wrap around. As shown in the bottom row, some damping is required. To summarize, we found that for the types of models discussed in the following the optimal way to compute  $P_{n1}$  synthetics is to use a time series of 1024 points, a Nyquist frequency of 2.5 hz, WF2 and an  $\alpha$  value of .0028 hz.

Numerical Experiments Figures 4 and 5 demonstrate that the short period waveshape of  $P_{n1}$  is relatively stable up through the first ten seconds after the onset of high amplitude signal after  $P_n$ . We discuss here a few numerical experiments designed to elucidate the composition of this signal and its sensitivity to details of the crustal structure. We begin with generalized ray calculations in the Helmberger and Engen (1980) layer over a half space crustal model. We have computed a section of displacement Green's functions for an isotropic compressional source and show the result on the left of Figure 11. We included 254 rays in the calculation corresponding to all paths with three or less reverberations in the crustal layer. Helmberger and Engen (1980) show the build up of the responses as up to 4094 generalized rays are successively added in corresponding to 5 reverberations in the crust, and generally speaking the next two levels of reverberation do not contribute significantly to the time window of interest here.

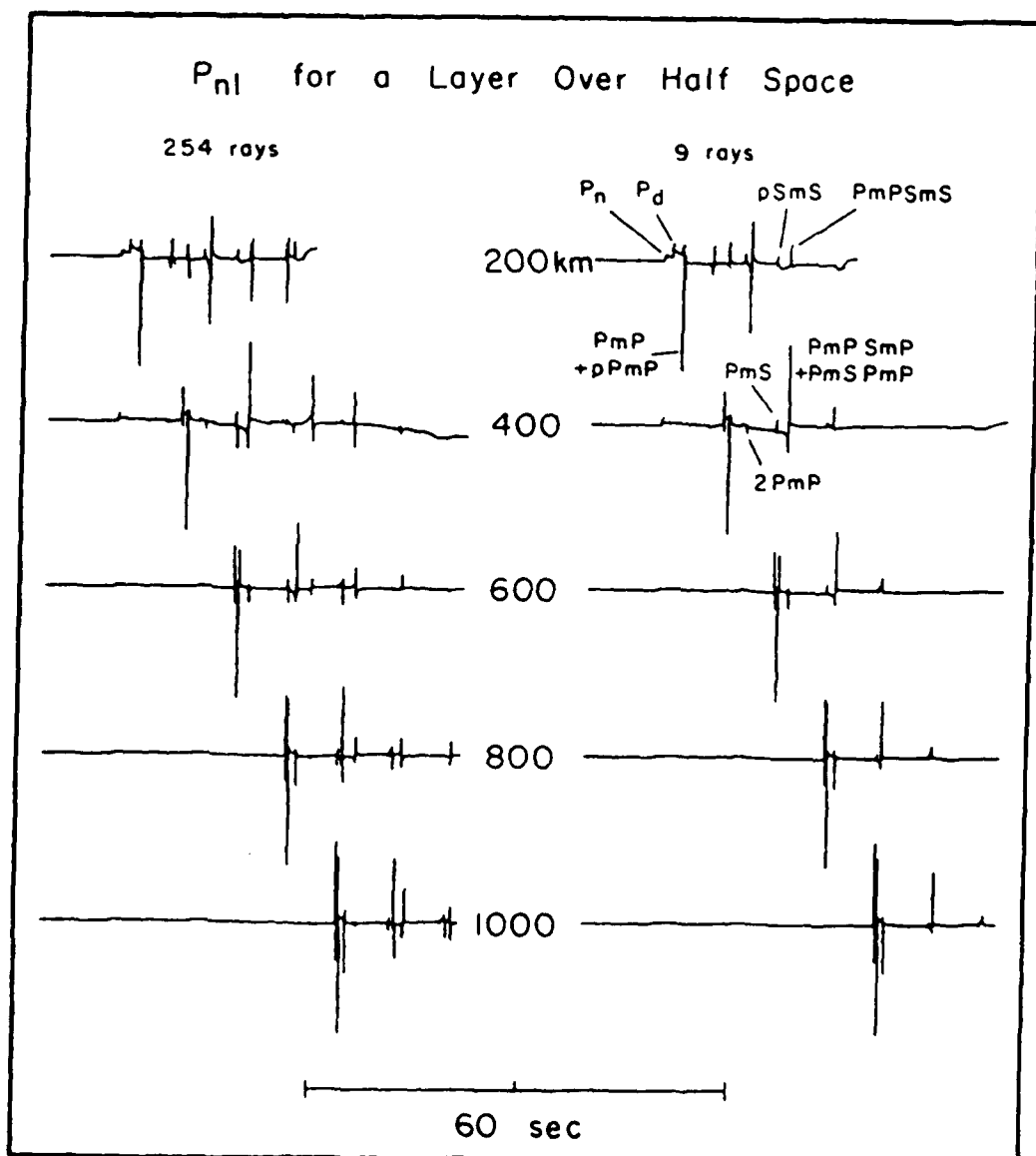


Figure 11. Broadband seismograms to show amplitude responses of individual rays computed by GENRAY88 (generalized ray theory) using a layer over half-space model of Helmberger and Engen (1980). Major contributing generalized rays are identified in the suite of right most seismograms.

The high amplitude portion of the responses appears to consist of a rhythmic sequence of sharp pulses which, judging from their complexity of shape, are probably the result of several different generalized rays. We have examined the response to small subsets of rays to attempt to identify which paths contribute the primary energy to these pulses. We found, as might have been expected, that the rhythmic sequence is related to successive orders of crustal reverberation with one relatively interesting complexity. A response section built from only 9 rays which appear to contribute most to the energy to the beginning of the Green's function is shown on the right of the figure. As indicated there, the first high amplitude pulse is made up of the post critical mantle reflection PmP, the direct ray noted as  $P_d$  and pPmP. The step-like  $P_n$  wave is identified separately, but in a generalized ray sense it is part of the PmP ray. The second reverberation of PmP is indicated in the diagram as 2PmP. It does not contribute significantly to the second high amplitude resonance pulse. This pulse is composed primarily by PmPSmP and PmSPmP. In other words, the second high amplitude spike is caused by rays with at least one converted leg. The pSmS and PmPSmS follow this high amplitude spike. The PmS phase precedes the spike. The later resonances seen in the complete responses on the left of the figure are due to similar complex groups of rays which arrive closely in time. Some of the results regarding the timing and amplitude associated with the contributions of certain converted rays in a layer over a half space are counter intuitive because the rays follow very asymmetric paths. S legs are almost vertical and P legs are relatively flat. The amplitudes of the rays are controlled by the ranges at which critical angle occurs.

There are two points we intend to make through this exercise. The first is that factors which might tend to change conversion coefficients and travel times of converted phases should be important in understanding the onset of high

amplitude signal we are trying to model in this work. The second is that the very beginning of this signal may properly be referred to as PmP, though the details of propagation of this energy will be much more complex in a realistic crust model than in a layer over a half space.

To begin our investigations into the behavior of  $P_{n1}$ , we designed several simple test models which had some of the major features one would expect to see on average in a real crust. They are shown in Figure 12. The first 5 models are of a surface gradient. Model 1 has a velocity decrease of about 20% in P and 30% in S over a range of 6 km in depth on top of the standard one layer model. The Green's functions for the one layer model and Model 1 are compared in the left two columns of Figure 13. The ranges shown are representative of those at which we have actual observations. The effect of the simple gradient is very pronounced at high frequency. The response with the surface gradient present is much more complex and apparently higher in frequency. The primary reasons are that the free surface reflection coefficients change substantially along with the timing of rays. In the one layer model, the conversion of P to S energy (rays like pS) is much stronger, whereas in Model 1 more energy stays in the compressional mode (rays like pP). In model 2, we experimented with an additional substantial drop in the P velocity with the S velocity fixed. In model 3, we did the reverse. The Green's functions did not change substantially in shape as illustrated in the right two columns of Figure 13. We therefore infer that the waveform results are not strongly sensitive to the ratio of P to S velocity in the crust gradient. Amplitudes vary by about a factor of 2. Models 4 and 5 represent progressively stronger gradients in both P and S and will be discussed further in the following. The Green's functions shown in Figure 13 were computed over a frequency range extending up to 5 hz. The data we wish to model has been filtered and convolved with the long period WSSN instrument

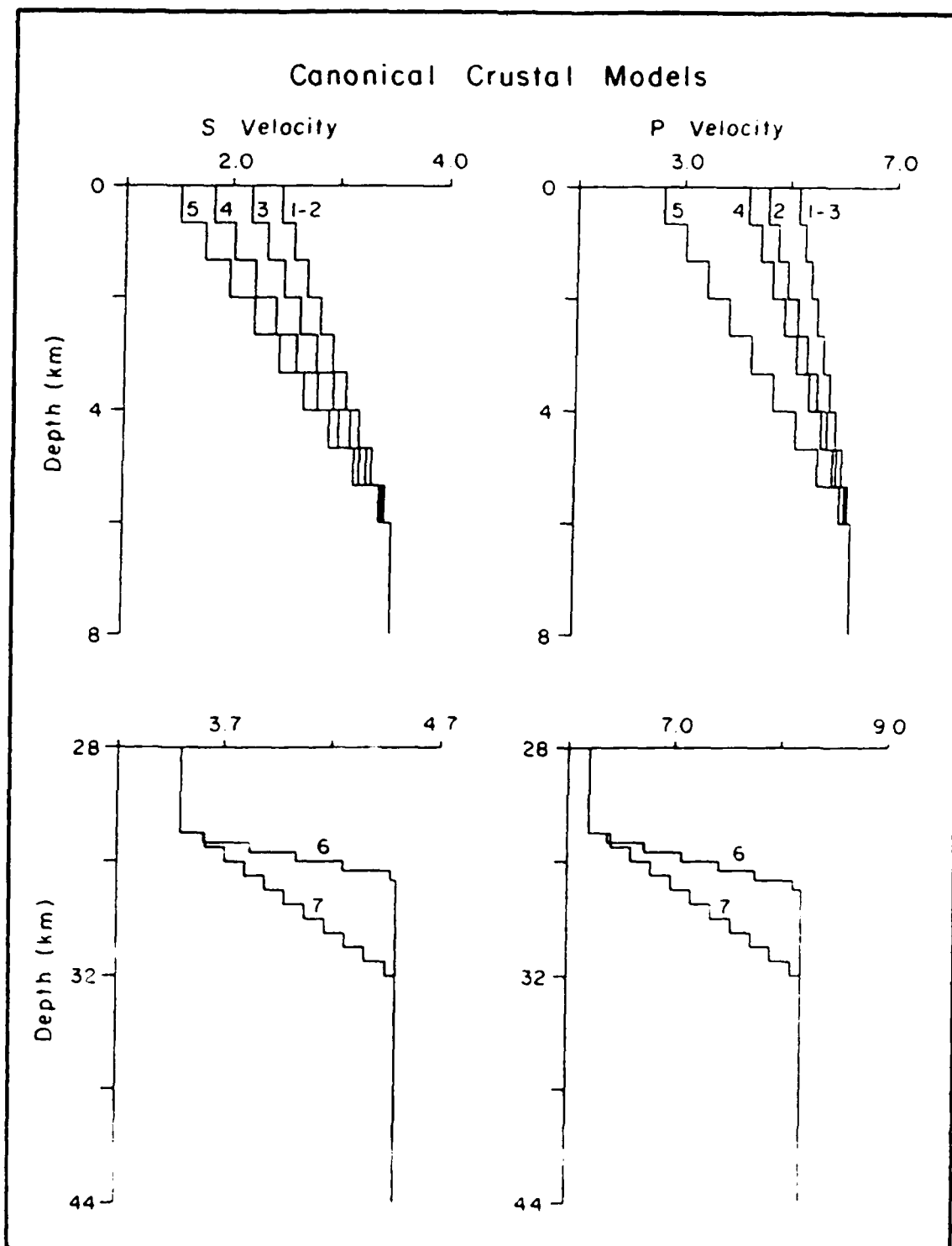


Figure 12. Canonical crustal models. Top two panels show the variation of P and S wave velocities within the upper 8 km of the crust (models extends up to 32 Km. Half-space P and S velocities are 8.2 km/sec and 4.5 km/sec). The lower two panels show the structure across the Moho discontinuity. Models 1-3 are for the perturbation study discussed in the text.

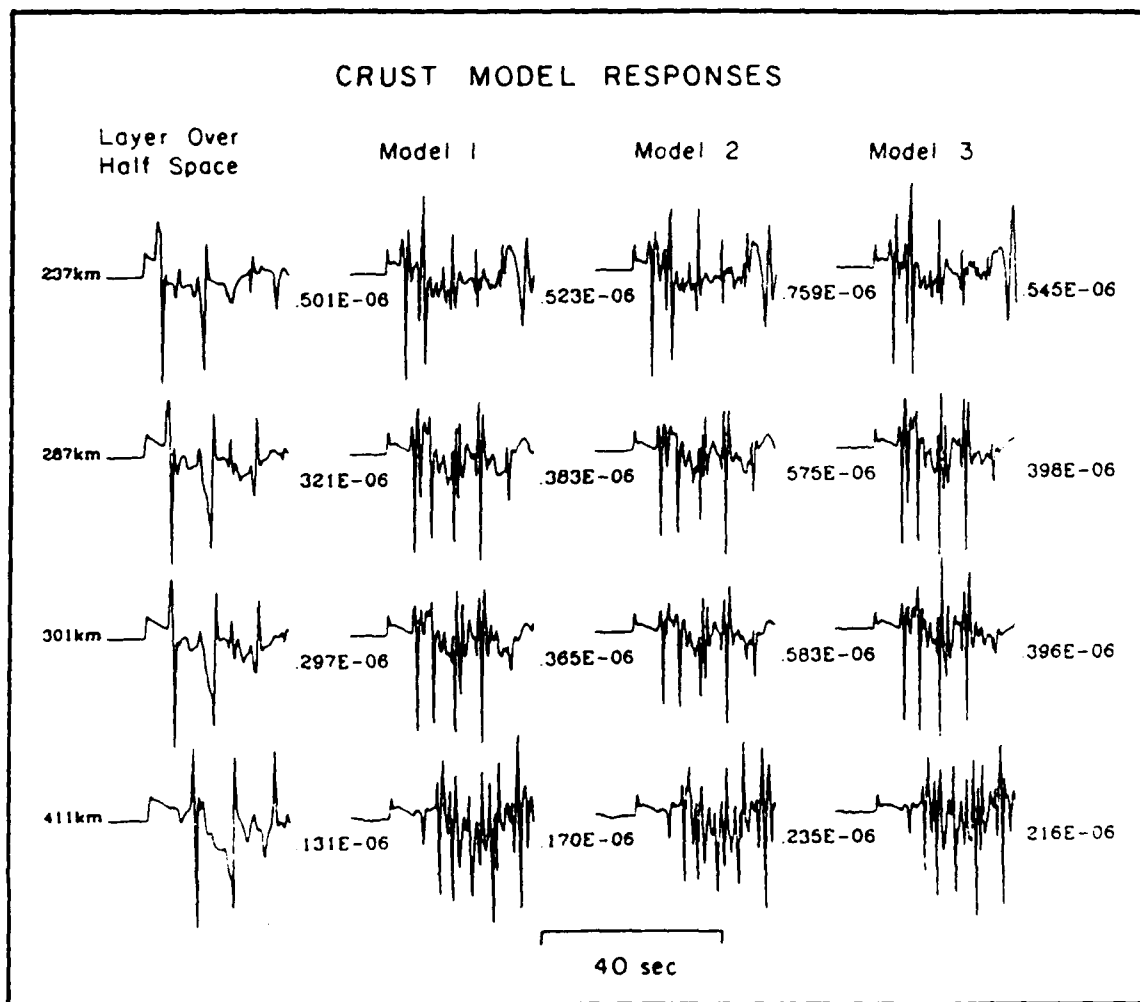


Figure 13. Broadband  $f$ - $k$  seismograms with a Nyquist of 5 Hz computed for models 1-3 including a layer over half-space model. All seismograms were convolved with a Mueller-Murphy source. The effects of the upper crust can be clearly noticed in the change of the frequencies and complexity of the waveforms.

response. It contains little energy at frequencies higher than 1 Hz. To confirm that it is important to account for the surface gradient in our modeling, we convolved the Green's functions with the instrument response. The results are shown in Figure 14. The arrangement of the columns is the same as in Figure 13. The surface gradient continues to be important in the lower frequency band.

We next examined the effects of a gradient at the crust-mantle interface. We computed synthetics at the same ranges for models 6 and 7 in Figure 12. The velocities above and below the interface are assumed to be constant. We found that the effects of the gradients were not significant at the level of the scatter in the waveform data and certainly not nearly as important as the surface gradient. The Green's functions for models 6 and 7 are compared to those for the one layer model in Figure 15 and with the WWSSN response in Figure 16. A gradient at the Moho must certainly have significant effects on waveforms at some ranges, particularly when the first arrival is triplicating through it. This occurs at around 150 km in the western U.S. The closest range from which we have data is 237 km, so all of the energy near the onset of  $P_g$  is well past critical angle and strongly trapped in the crust. This explains its insensitivity to the details of the crust-mantle transition zone. The results of these numerical experiments also depend on how realistic the models we tested are. In fact, we selected them based on previous estimates of the strength of the surface and Moho gradients. Figure 17 compares our model 4 to the Pahute Mesa crust model of Hartzell et al. (1983). In fact they are very similar, and, as we shall show in the following, this model is very consistent with the data. On the right of the figure, we show a model developed for the crust-mantle transition for the path from NTS to Las Vegas. This work is discussed in the final section of this report. This realistic gradient model is very similar to our model 7.

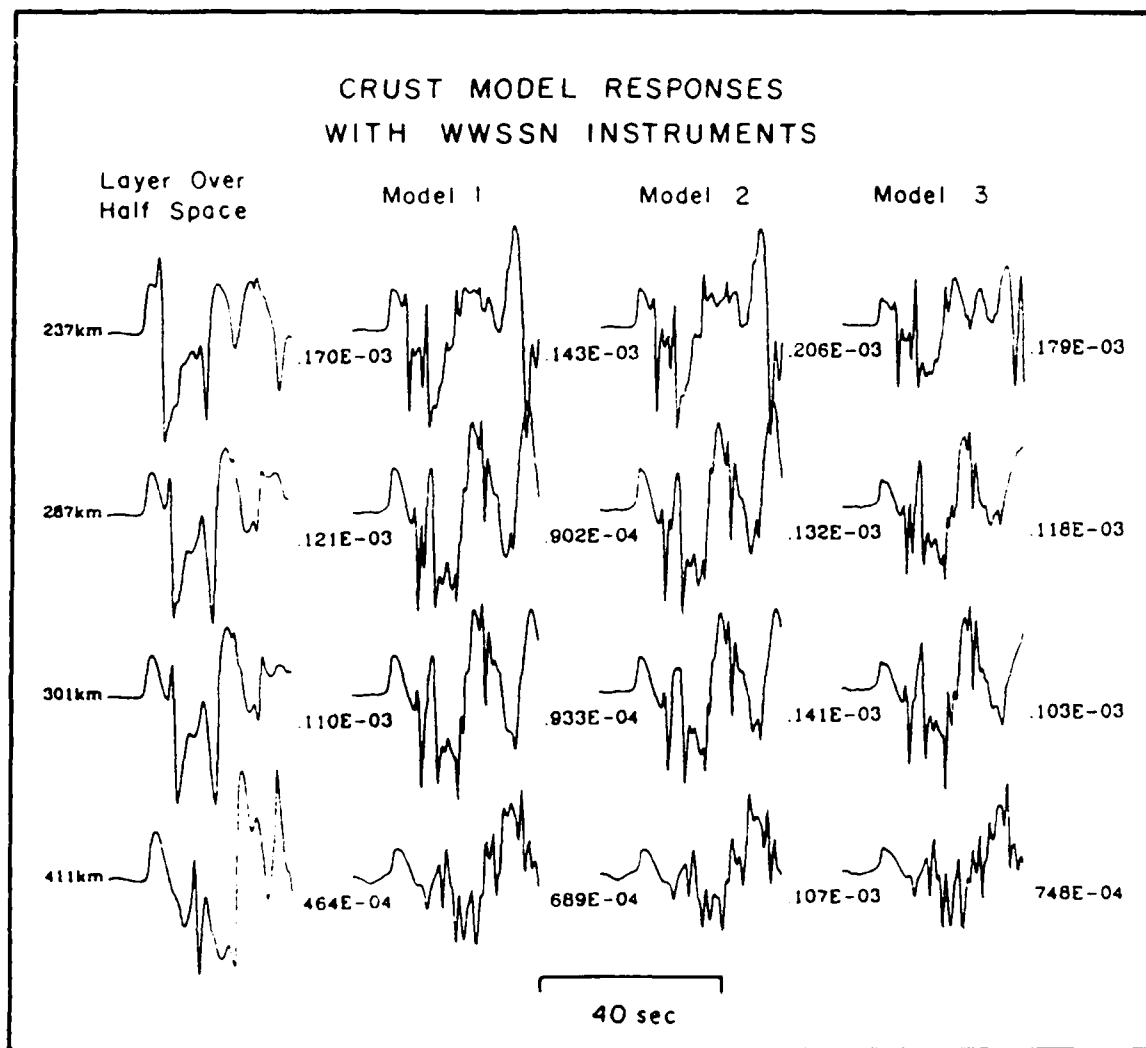


Figure 14. Same seismograms as shown in Figure 13, but after convolving with a long-period WWSSN instrument.



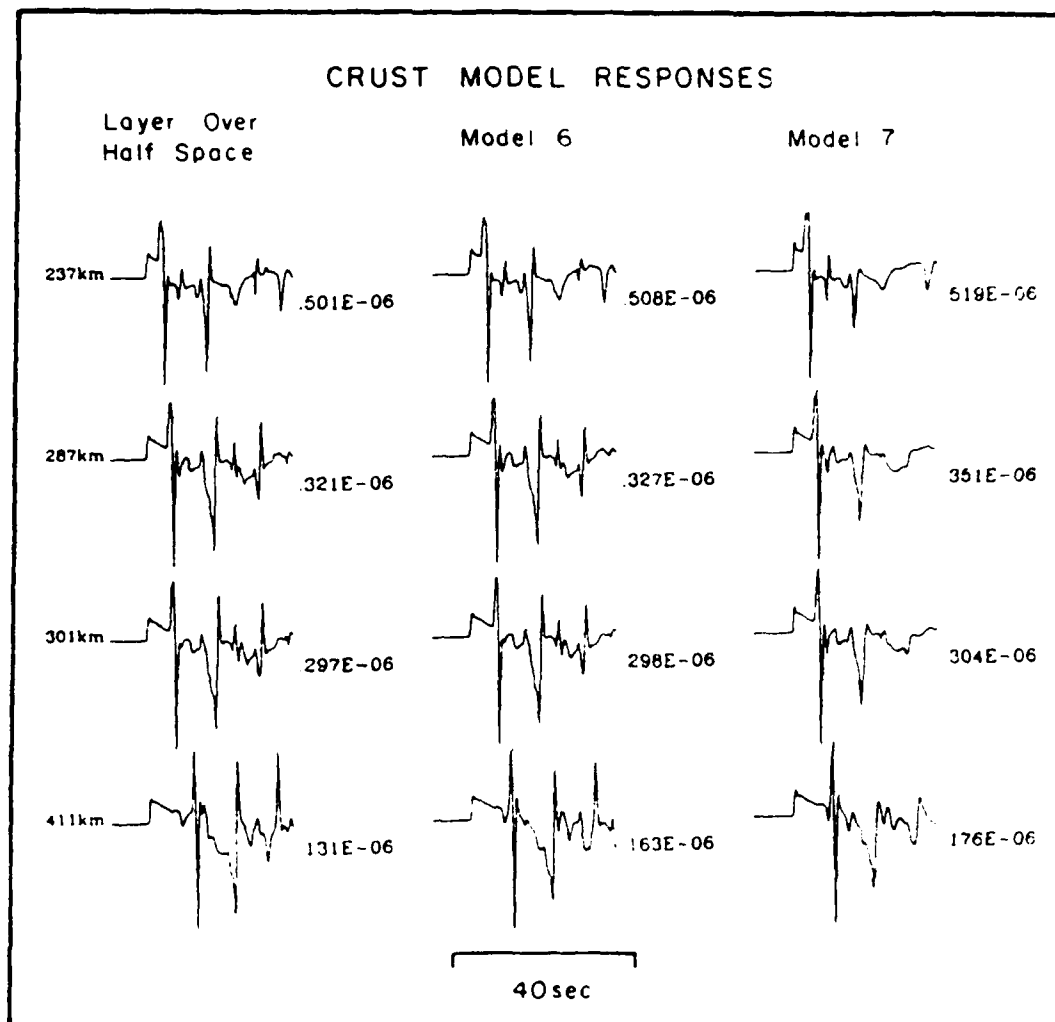


Figure 15. Broadband  $f-k$  seismograms with a Mueller-Murphy source function computed using a transition zone 3 km thick crust across the Moho discontinuity in the Helmberger and Engen (1980) crustal model. The effect can be seen in the changes of the relative amplitude of phases.

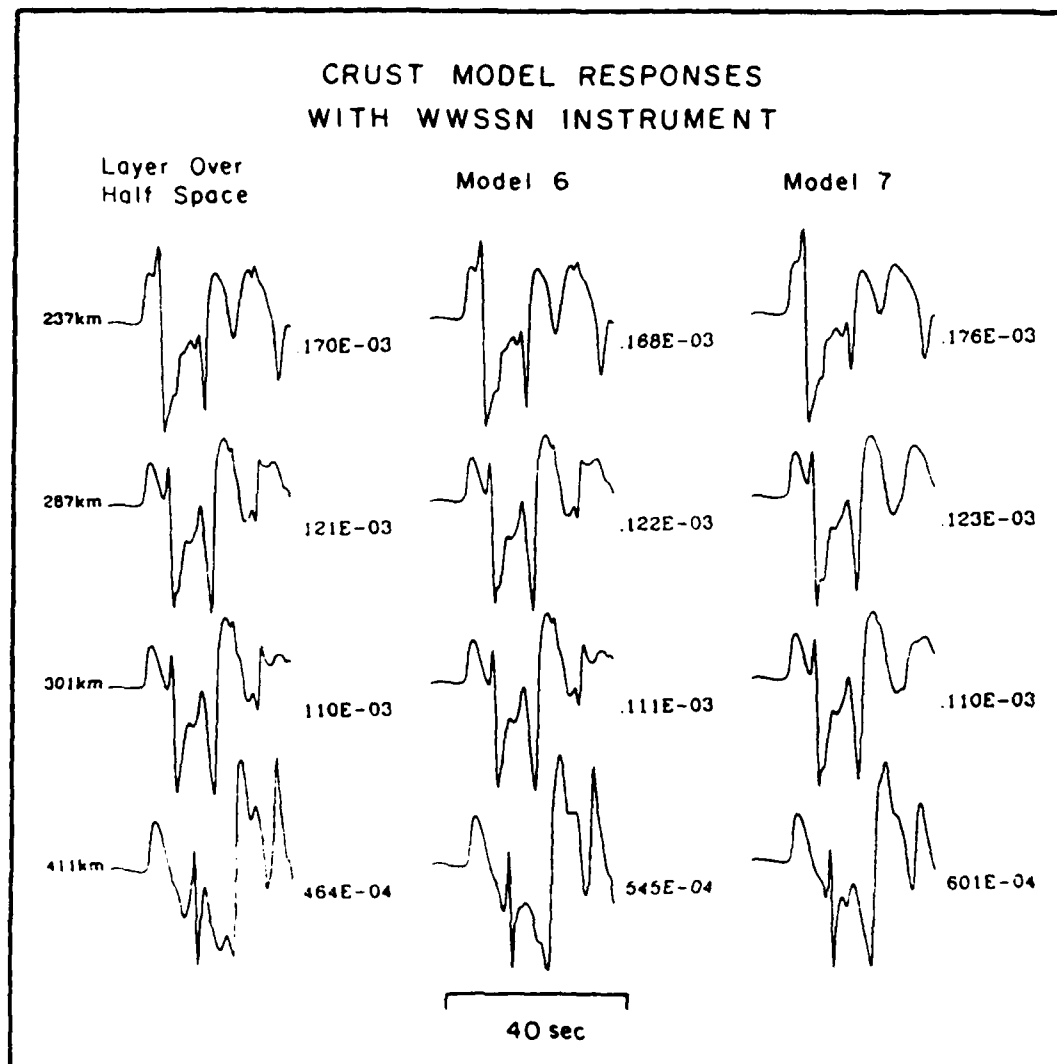


Figure 16. Same seismograms as shown in Figure 16, but after convolving with a long-period WWSSN instrument. The effect of the transition zone is small.

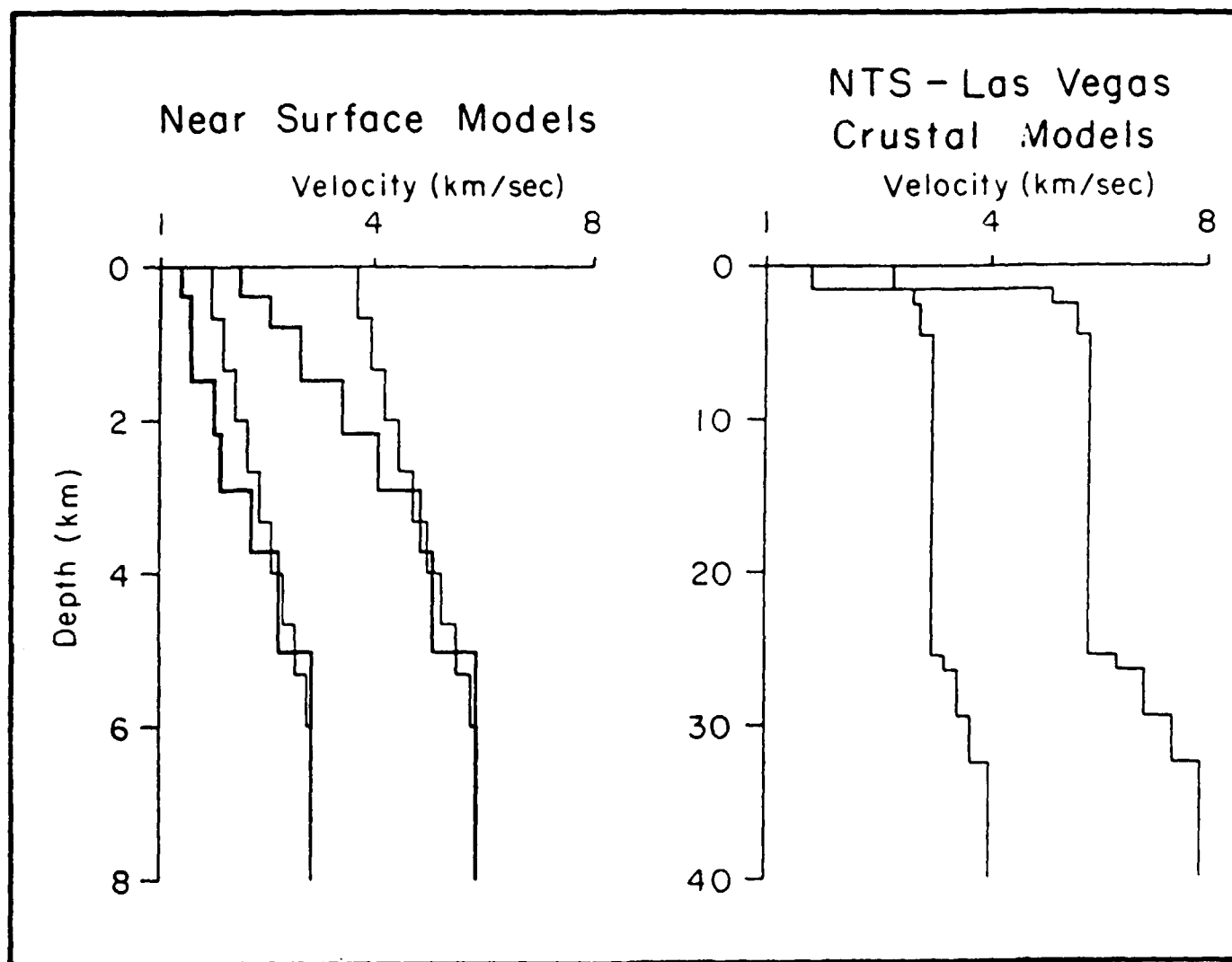


Figure 17. Crustal Models with both P and S wave velocities. On the left are our preferred model 4 and Hartzell *et al* (1982, dark lines) and on the right is a crustal model developed from NTS to Las Vegas.

MODELING RESULTS We proceeded then with the assumption that the most important portion of the crust model to adjust was the lid gradient in order to improve the fit to short period  $P_{n1}$ . Since our numerical experiments indicated that the ratio of P to S velocities was not important, we tested the effects of increasingly intense crustal gradients. We refer to the layer over a half space model as model 0 and the increasing gradients as models 1, 4 and 5 as illustrated in Figure 12. The results of the experiments are shown in Figures 18 through 21. For each of the eight stations, the data is shown at the top and the synthetics for each of the four models below.

As our numerical experiments would have indicated (see Figure 13), addition of the surface gradient causes a notable increase in the amount of high frequency energy. Model 0, the layer over a half space, is obviously too long in period to satisfy the observations. This is particularly apparent in the first arriving energy or  $P_n$ . The effect of the weakest gradient model, model 1, is not strong enough and the synthetics are still too low frequency. The gradient model 4 predicts approximately the correct frequency content, and its synthetics are shown directly beneath the data. It provides some remarkable waveform fits to  $P_n$  and the onset of PL. The model 4 results are shown by themselves in Figures 22 and 23. Data is shown in dark line over the synthetics below. Some of the more notable fits are to ELK from JORNADA, KNB from GIBNE, ALQ from KAPPELI and JAS from JORNADA. It is important to emphasize that a single vertically stratified model has been utilized to fit all of the data. No doubt strong lateral variations exist, and we could have obtained a better fit by using a separate model for each path. However, our main point here is to prove the efficacy of using relatively simple models to predict the beginning of  $P_{n1}$  down to periods as short as 2 seconds.

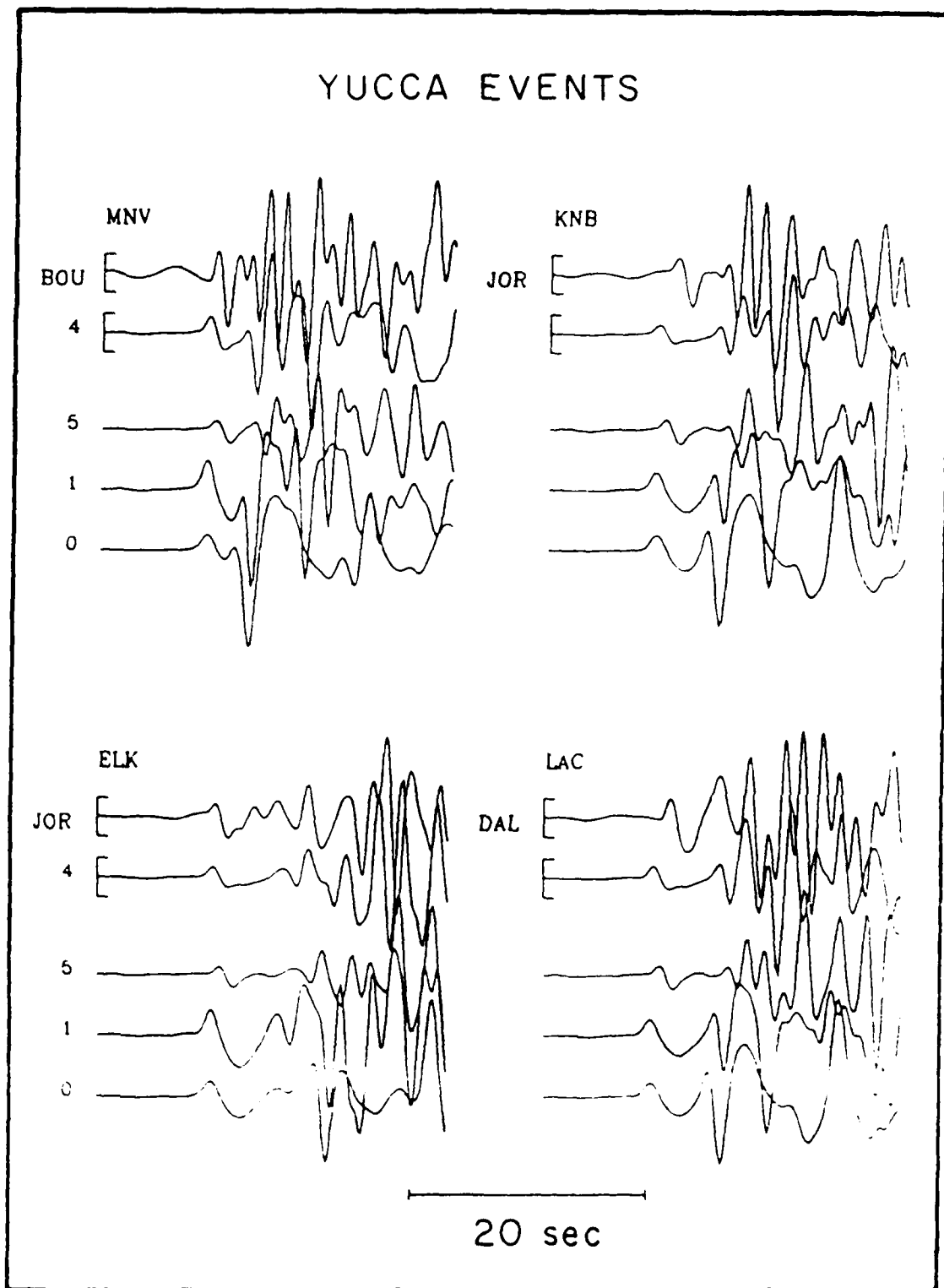


Figure 18. A comparison between data (top seismogram) and synthetic seismograms computed from four canonical crustal model. The comparison is made for Yucca flat explosions at four LLNL stations.

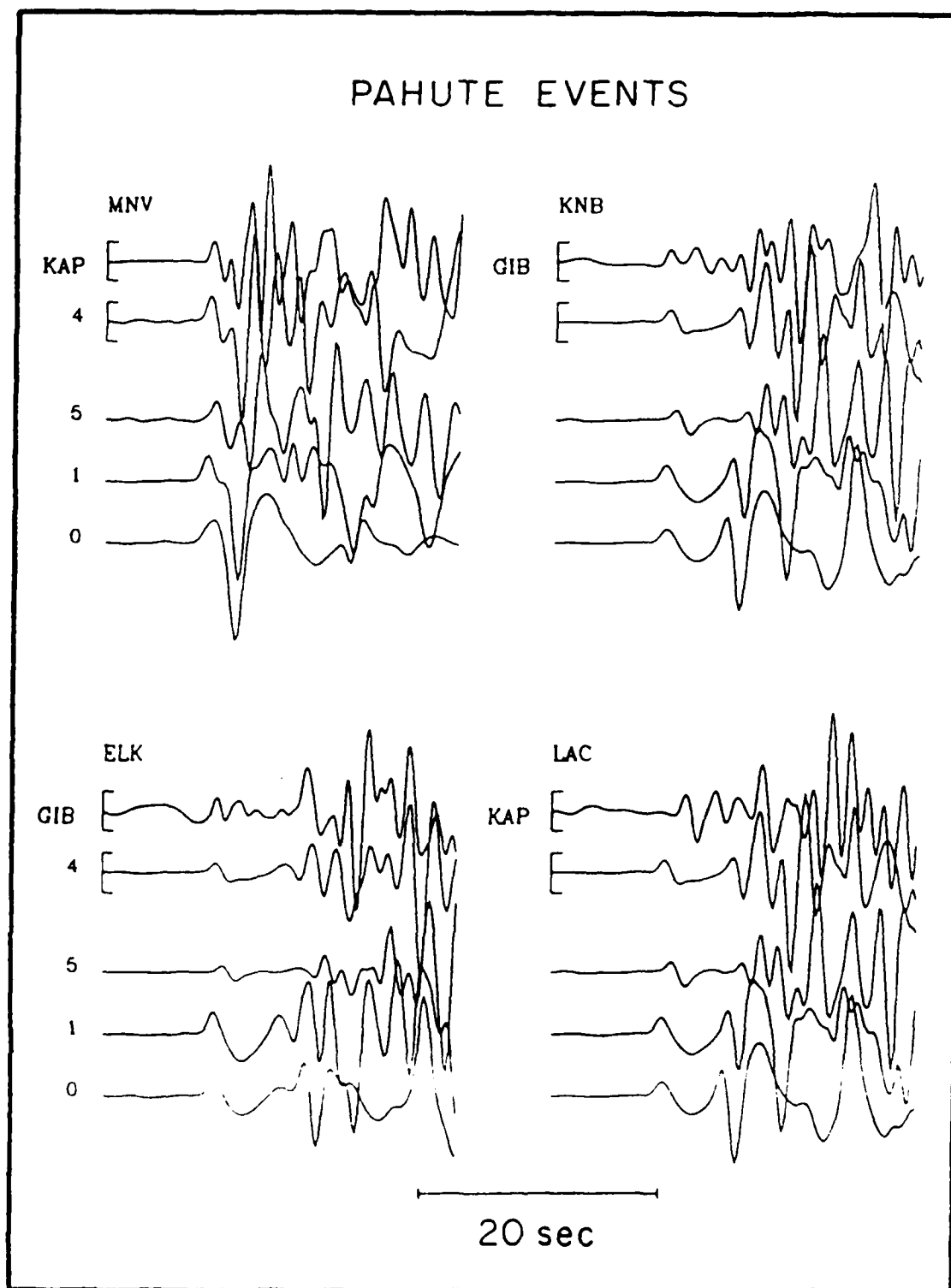


Figure 19. A comparison between data (top seismogram) and synthetic seismograms computed from four canonical crustal model. The comparison is made for Pahute Mesa explosions at four LLNL stations.

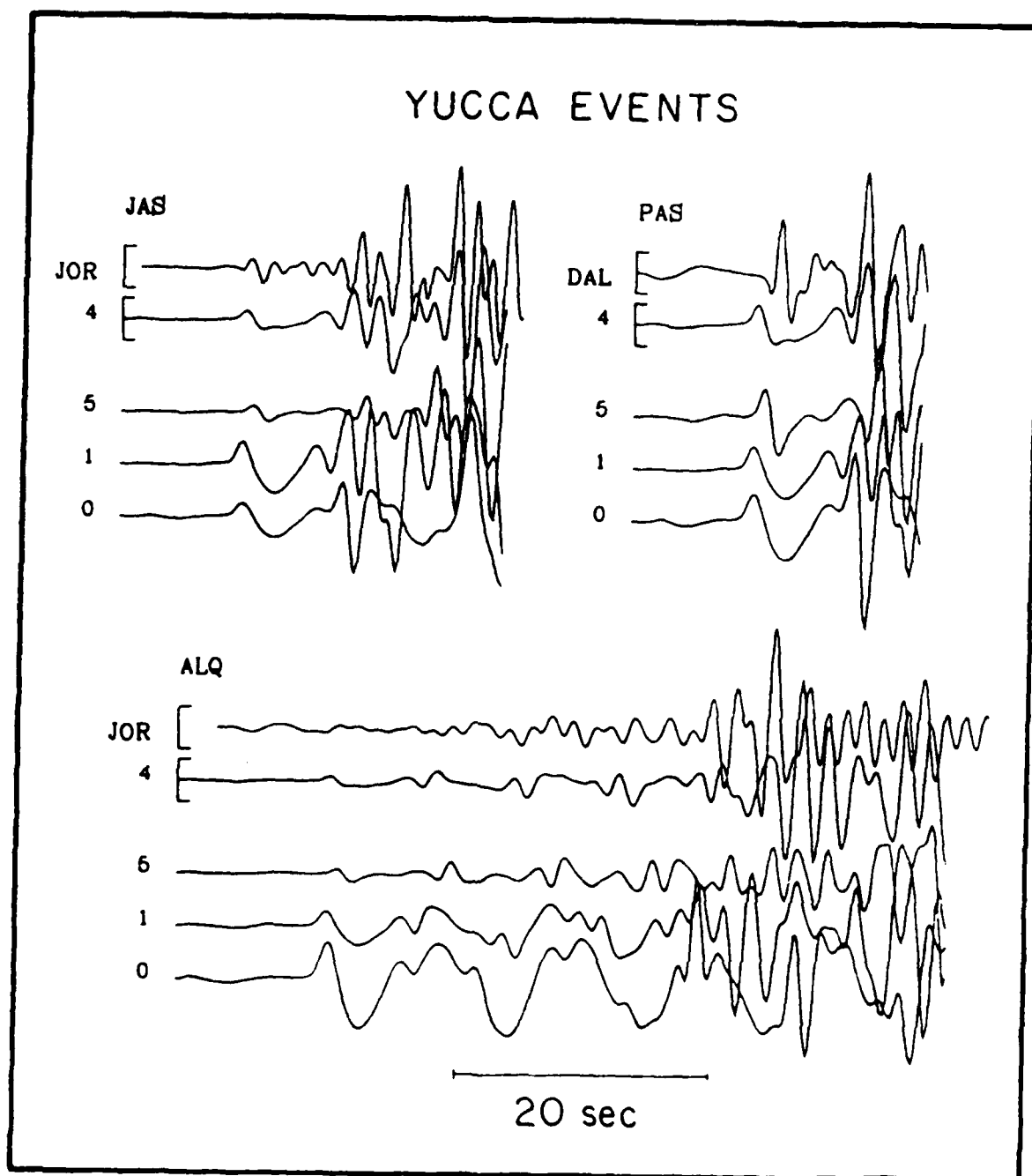


Figure 20. A comparison between data (top seismogram) and synthetic seismograms computed from four canonical crustal model. Comparison is made for Yucca flat explosions at four stations- JAS, PAS, PFO and ALQ.

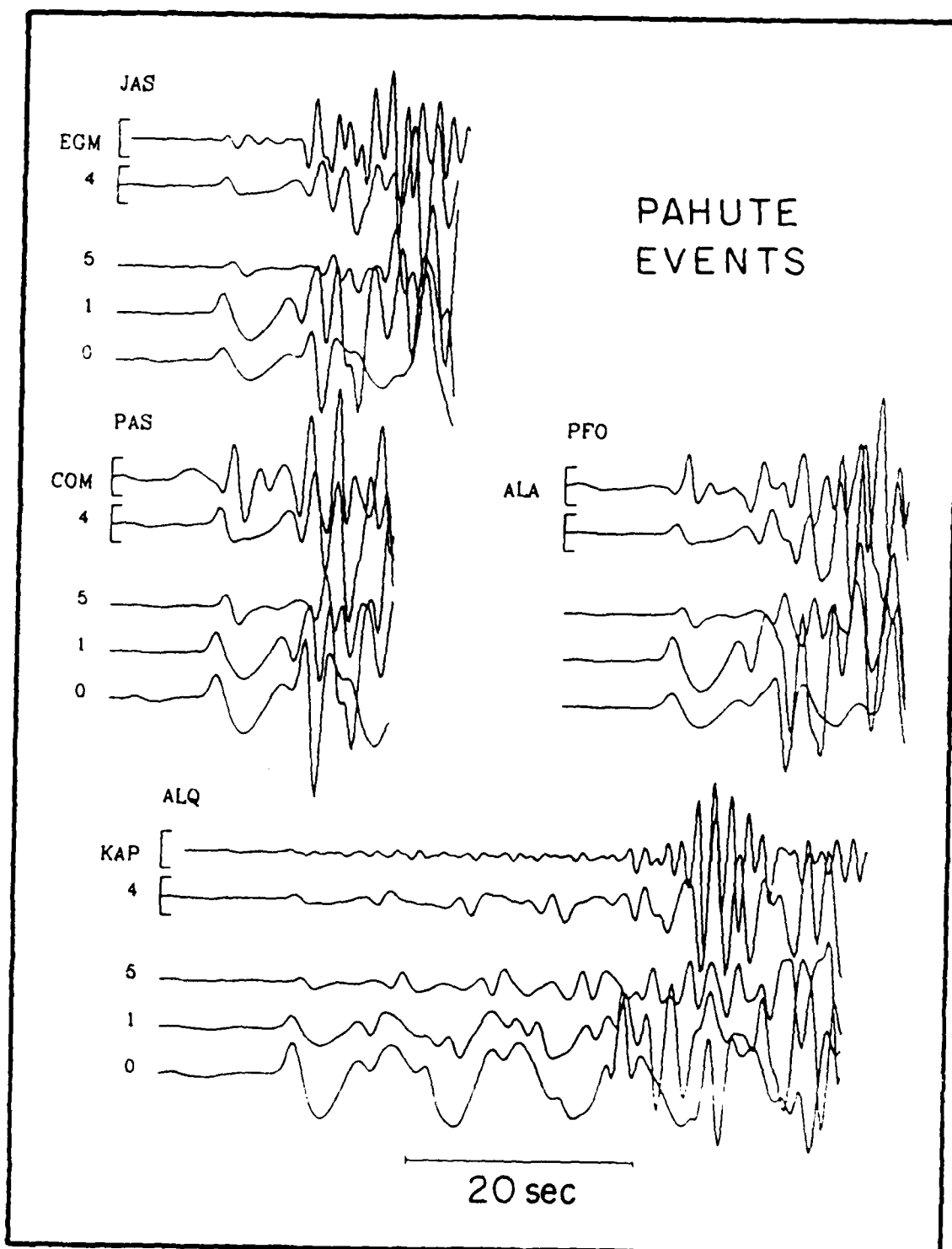


Figure 21. A comparison between data (top seismogram) and synthetic seismograms computed from four canonical crustal model. Comparison is made for Pahute Mesa explosions at three stations - JAS, PAS and ALQ.



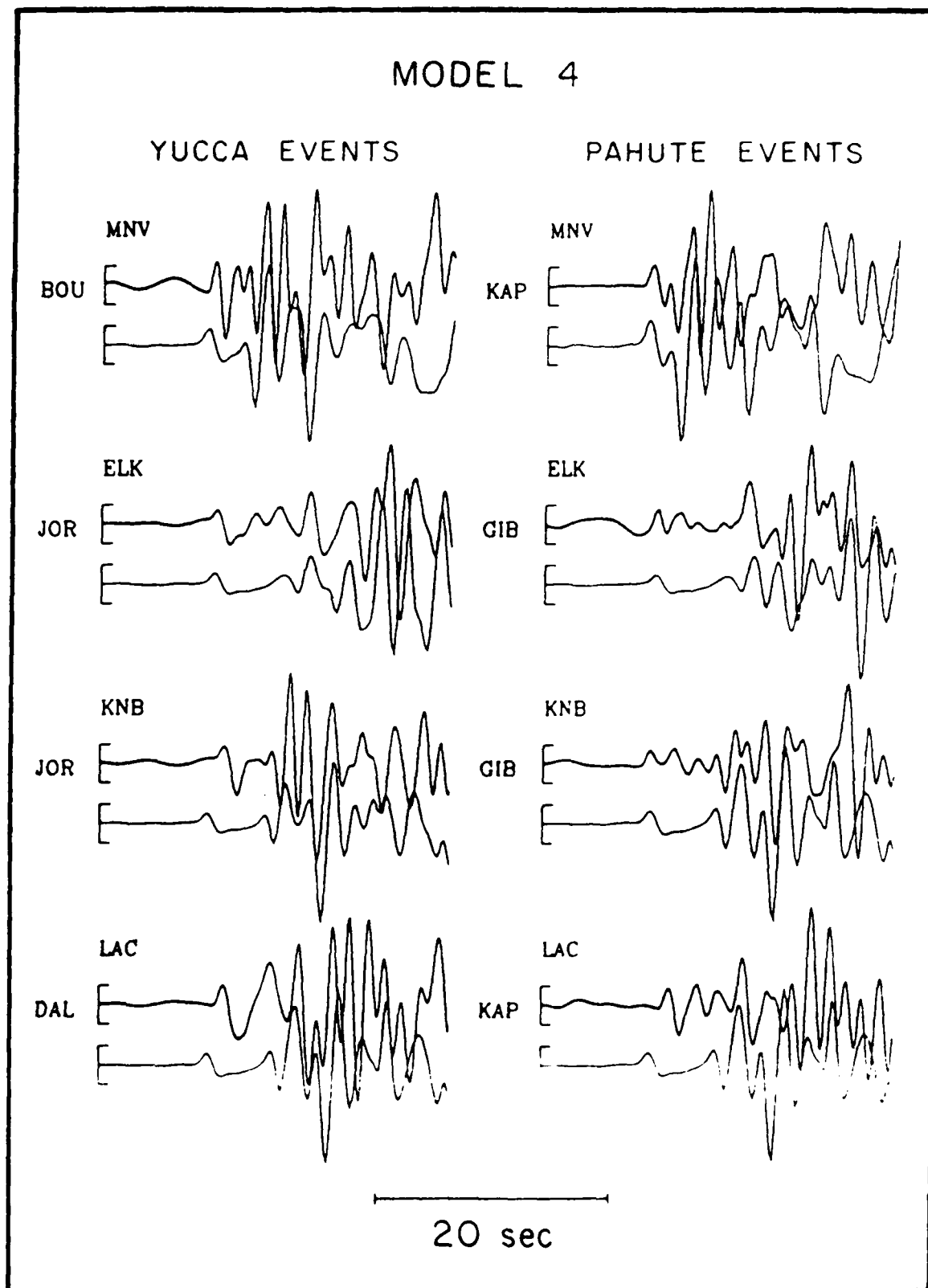


Figure 22. A comparison between the data (top seismograms) both from Yucca flat and Pahute Mesa and synthetic seismograms computed from our preferred model 4. The initial part of the synthetic seismograms shows remarkable correlation with data. The comparison is shown for the four LLNL stations.

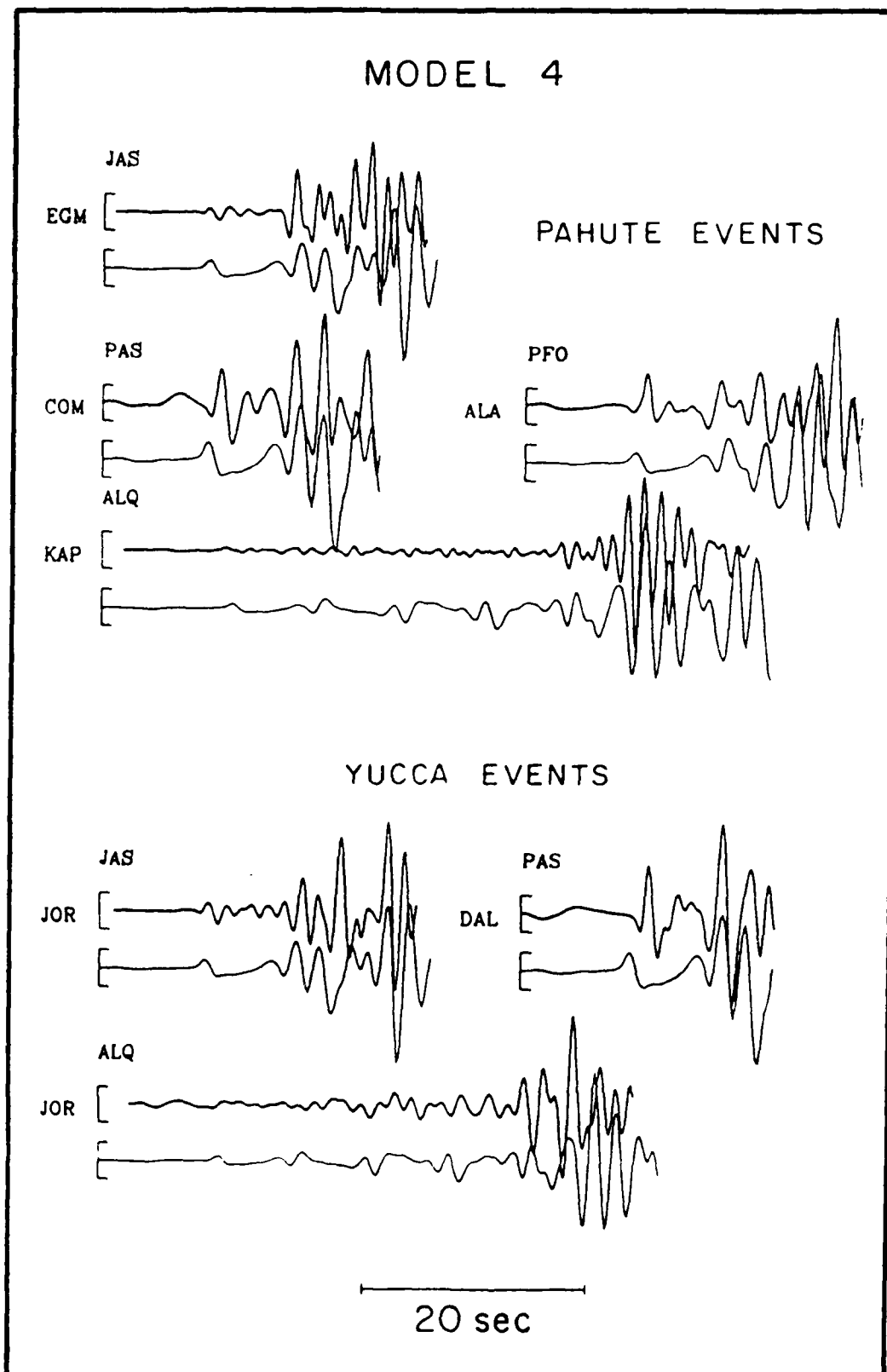


Figure 23. A comparison between the data (top seismograms) both from Yucca flat and Pahute Mesa and synthetic seismograms computed from our preferred model 4. Initial part of the synthetic seismograms shows remarkable correlation with data. The comparison is shown for the stations - JAS, PAS, PFO and ALQ.

### INITIAL WORK ON $P_n$ WAVEFORM DISCRIMINANTS

The most successful regional discriminant developed to date is based on systematic differences in the spectral content of explosion and earthquake sources (Murphy and Bennett, 1982; Taylor et al., 1988). Perhaps surprisingly, but nonetheless consistently, NTS explosions are reduced in levels of high frequency energy with respect to earthquakes of the same magnitude. There is, as yet, no physical explanation for this difference, so in spite of the success of the approach in the western U.S. there are serious questions to be answered regarding its applicability in other regions of the world. In reports two and three, we discussed the development of another somewhat less accurate, but more physically based discriminant which relies on the waveform of regional  $P_n$  waves. We will summarize the key results here.

Because of the results to be presented in the following section, we begin by emphasizing that the development of the regional waveform discriminant was rooted in past experience with waveforms of teleseismic P waves from nuclear explosions. Figure 24 is taken from Burdick et al. (1984). It shows observed and synthetic, long and short period records from the nuclear test, CANNIKIN. Arrows on the left of the figure draw attention to a subtle feature in the short period records which is associated with the arrival of the phase pP. The records where the feature appears are assumed to be along high Q paths ( $t^* = 0.8$  s). Along lower Q paths the feature washes out. The long periods are not affected by pP in a clearly visible way.

This previous experience with the effects of pP on teleseismic short period P waves proved valuable in interpreting regional  $P_n$  waveforms. When the digital signals from NTS explosions were averaged (as in Figures 3 and 4), it was observed that the average  $P_n$  waveform was very similar to those on the left of Figure 24 although much shorter in period. Average waveforms at 5 stations in the digital

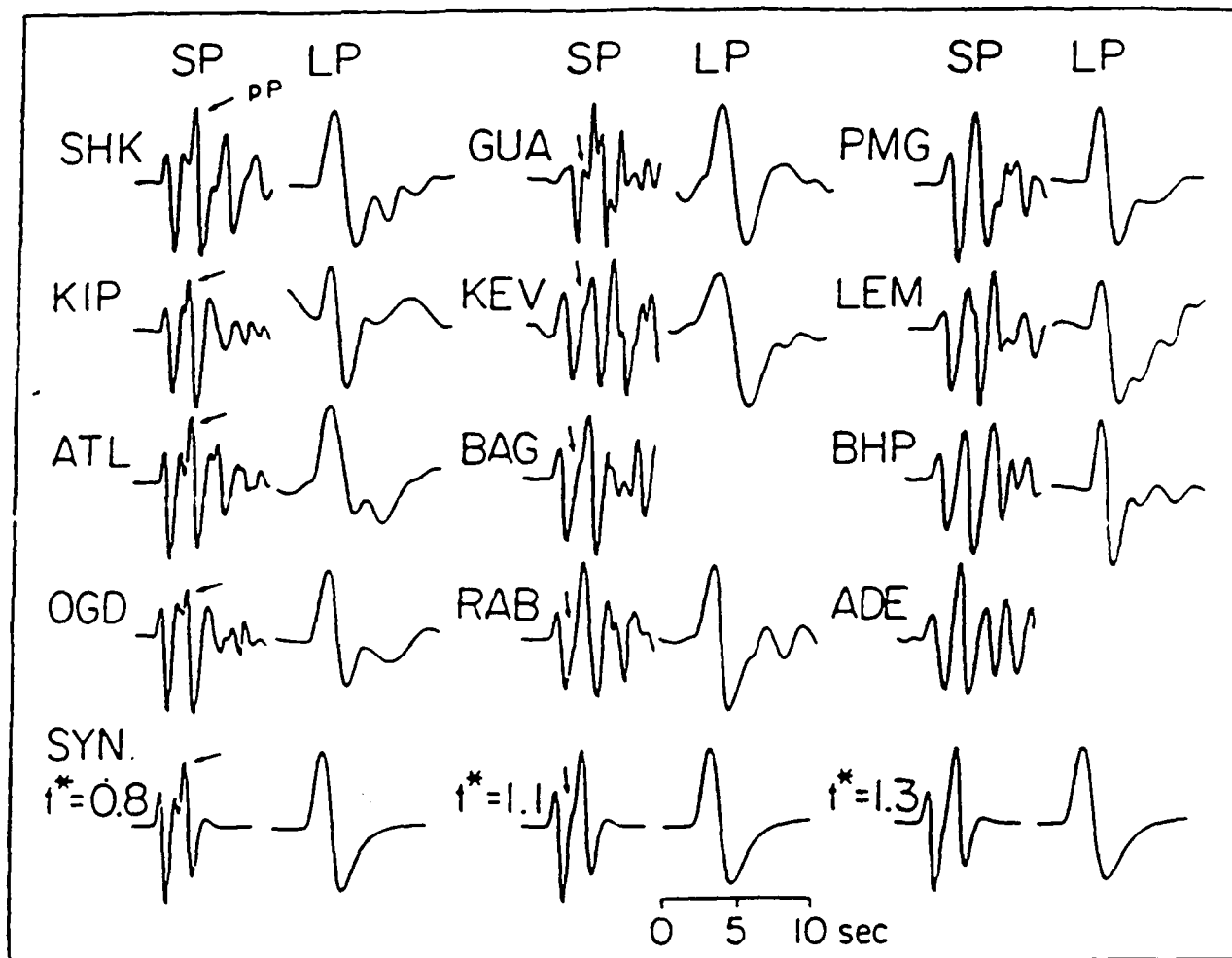


Figure 24. Comparison of observed short and long period  $P$  waves with synthetic for a range of  $t^*$  values at teleseismic distances. As  $t^*$  increases, the interference in the second upswing produced by  $pP$  becomes less apparent.  $pP$  can be observed as a distinctive double peak and is produced in the synthetics with an artificial delay.

net are shown in Figure 25. The consistent splitting of the second upswing is indicated by the arrows. The clear implication is that the physics of the wave propagation of short period teleseismic P and short period  $P_n$  is very comparable. More precisely, the interaction of pP with P must be similar in the two instances. This is not unreasonable in that the apparent velocity of  $P_n$  is about 8 km/s and that of teleseismic P only increases to about 12 km/s at 30°. The associated change in pP timing and amplitude is small. The implications for regional discrimination are clear. Only very shallow sources like explosions will have depth phases at very short times. Earthquake depth phases will be much later. To test the performance of this discriminant, we assembled a set of  $P_n$  waveforms from small earthquakes near NTS, windowed out the first three seconds of  $P_n$  and measured the correlation with the average  $P_n$  waveforms of explosions like those shown in Figure 25. A similar procedure was carried out on the explosion data base. The results from one station (JAS) are shown in Figure 26. The explosions are displayed as stars and the earthquakes as crosses. The separation of the populations is good enough to warrant more study of this discriminant.

The discrimination capability illustrated in Figure 26 only demonstrates that the  $P_n$  waveform of explosions is stable at JAS and consistently different from earthquake waveforms. However, the similarity of the waveforms in Figure 25 suggests that the shape of the explosion waveform is consistent from station to station. That this is indeed the case is shown in Figure 27 where the average JAS explosion waveform has been correlated with the explosion data base at MNV. Moderately good event discrimination is still possible. These studies suggest that one method to achieve discrimination with a regional net will be to continuously monitor the waveform of  $P_n$  onset at all of the stations and to test in an objective fashion for the presence of depth phases.

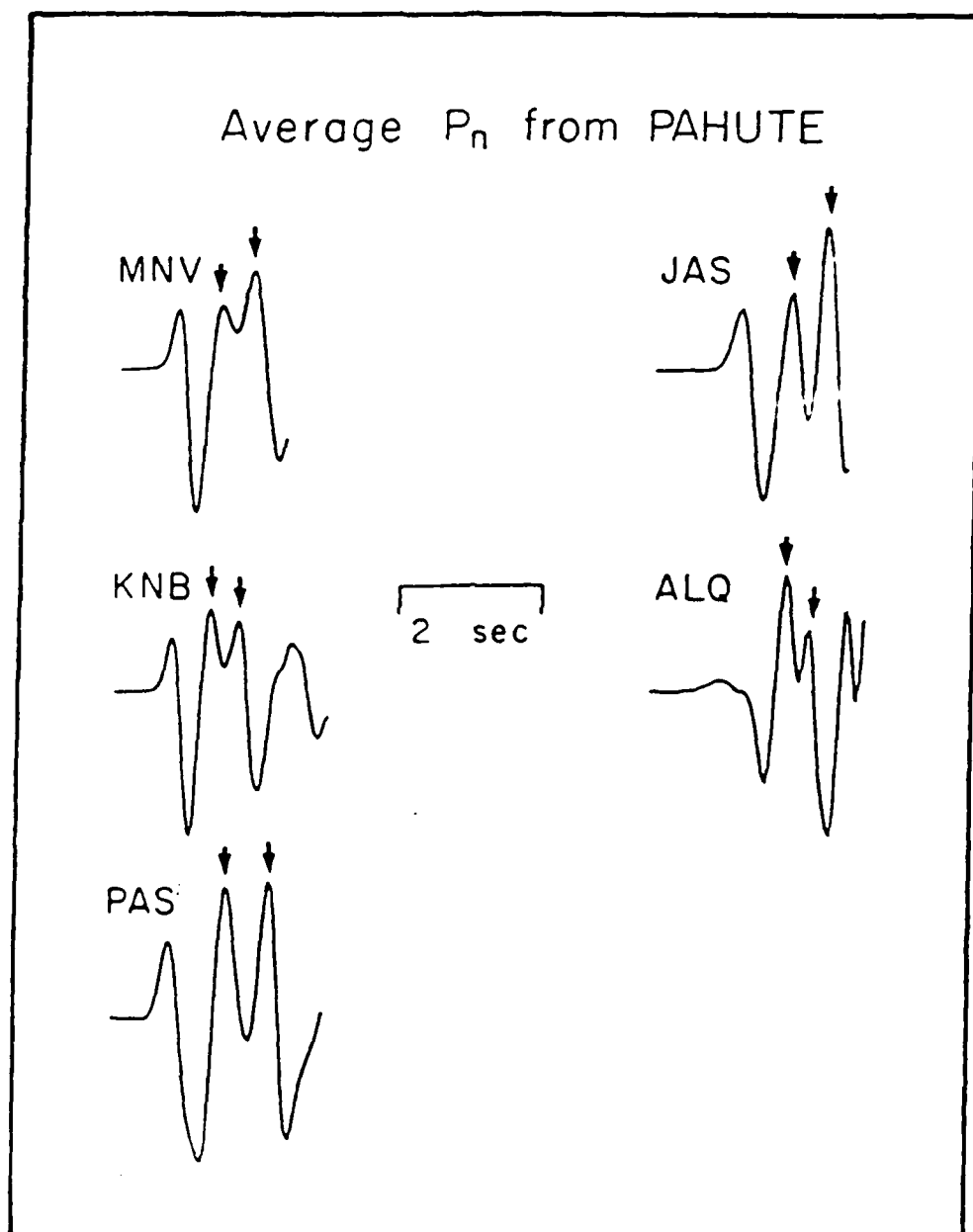


Figure 25. The average  $P_n$  waveform for Pahute explosions observed at stations in the western U.S. digital net. The split third swing is indicated by arrows.

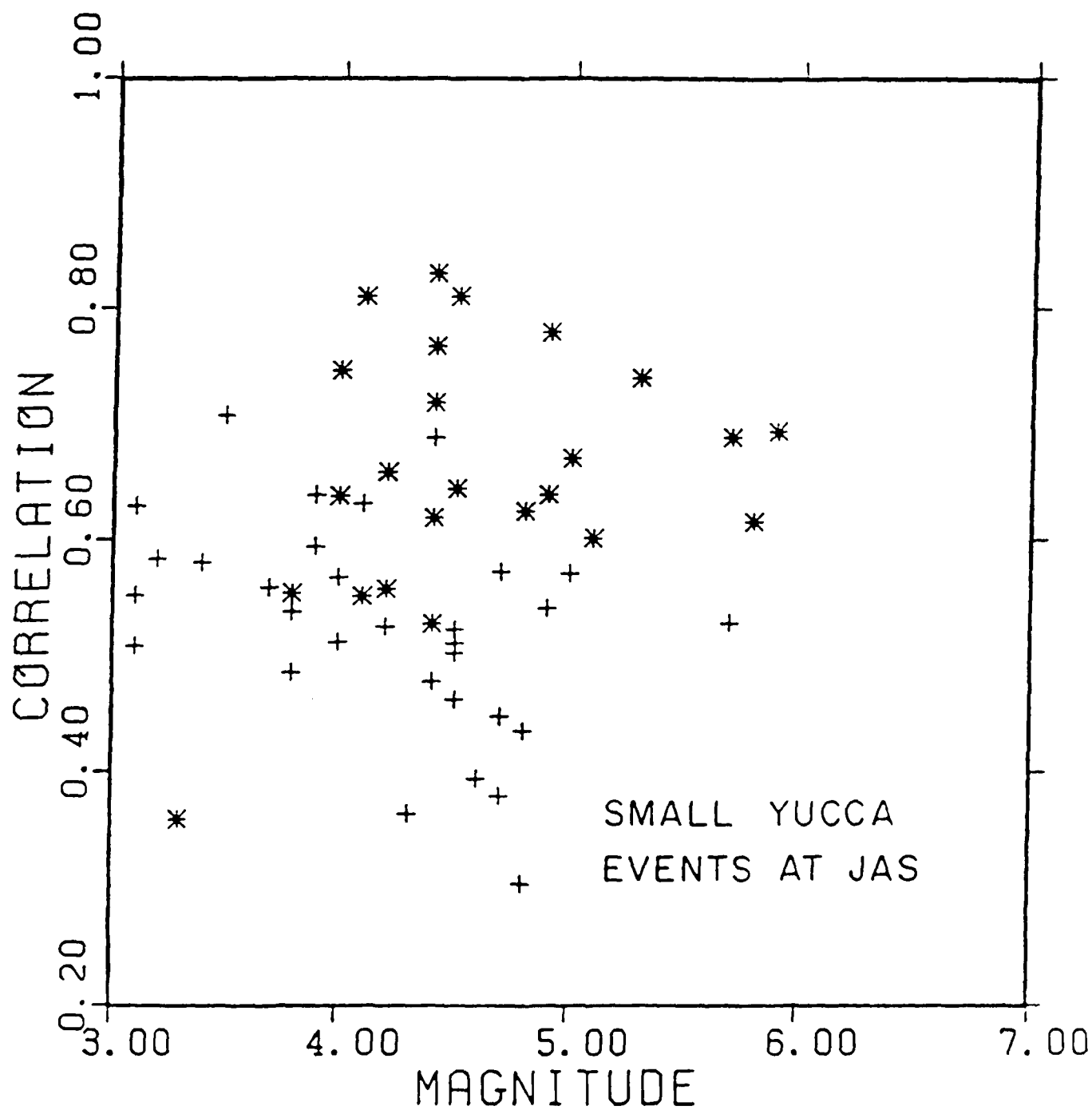


Figure 26. Discrimination of Yucca explosions from earthquakes using correlation with the average  $P_n$  waveform at JAS. The explosions are stars and the earthquakes are crosses.

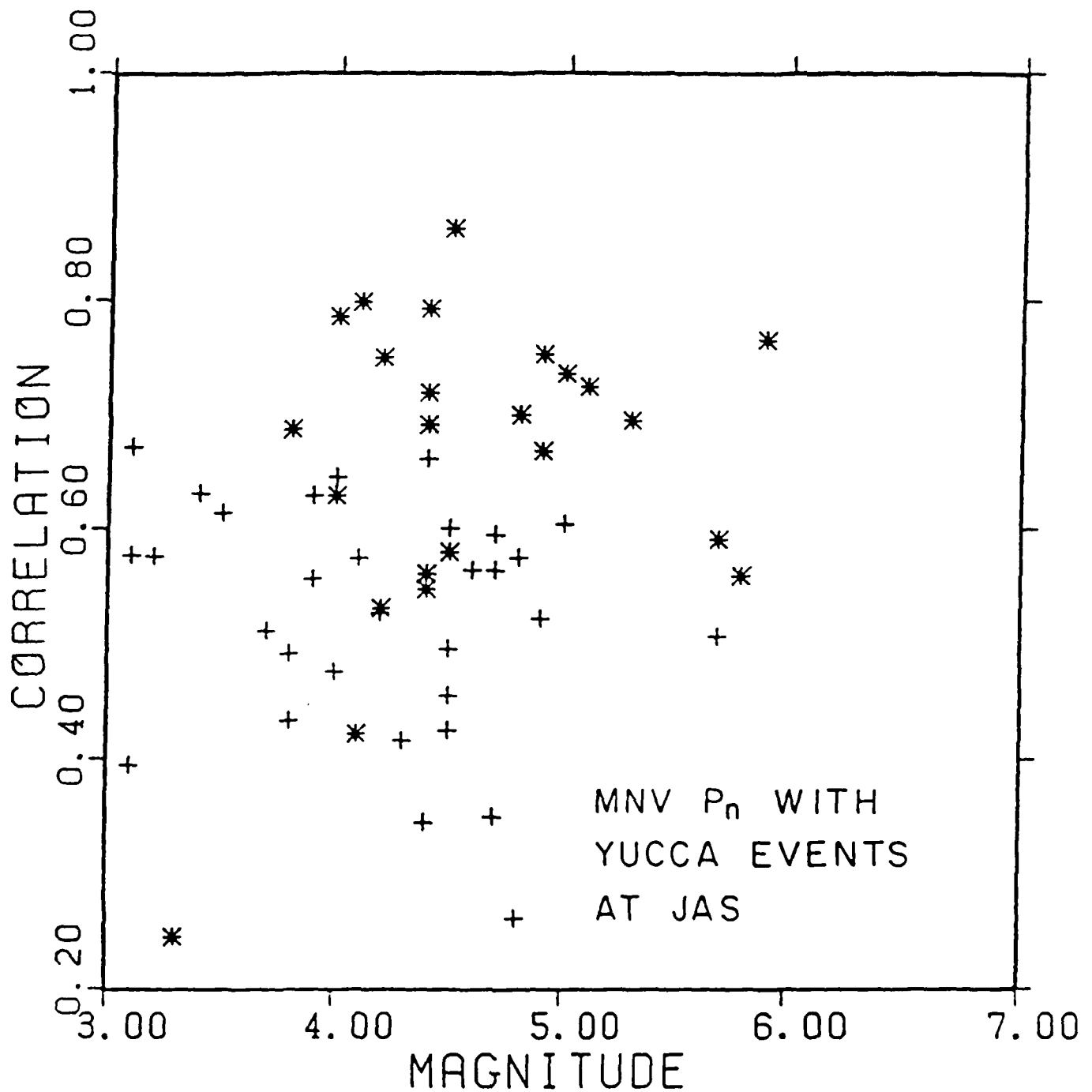


Figure 27. Discrimination of Yucca explosions from earthquakes using the average  $P_n$  waveform from MNV and the data base from JAS. Explosions are stars and earthquake are crosses. The separation of the populations is comparable to that in Figure 26 illustrating the transportability of the discriminant.



One final study from report 3 which needs to be reviewed here is a forward modeling study of the broad band  $P_n$  waveforms from the LLNL stations which was carried out. A typical result is shown in Figure 28 where the waveforms of four Pahute events as recorded at MNV are displayed. The data are shown as solid lines and synthetics for an appropriate crustal model and explosion source are shown as dashed lines. Because the instruments are broad band, deconvolving the response out is a stable operation which has been carried out. The traces shown are true ground velocity. The arrows indicate the arrival of  $pP_n$  in the data and synthetics. The observed  $pP_n$  is consistently much later than the elastic predictions. This discrepancy was observed for all events at all stations where the waveforms could be modeled. A similar result has been reported in most studies where  $pP$  times from nuclear tests have been measured. These results are relevant to the new work discussed next. More details of the investigation are available in the third report (Burdick et al., 1988).

### P<sub>n</sub> WAVEFORM DISCRIMINANTS AND SPALL

The work in the final quarter of this project on the P<sub>n</sub> waveform discriminant has been directed at developing a further appreciation of the physics behind it. We have examined the conclusion from report 3 that the P<sub>n</sub> at regional distances appears more like a turning ray in a smooth positive gradient than a true head wave on the crust mantle interface. To accomplish this, we have modeled the transition of P<sub>n</sub> from a second to a first arrival. We found that the Moho under NTS behaves much more like a smoothly graded structure than a sharp discontinuity. We have also developed a physical explanation for the apparent delay of pP<sub>n</sub> as illustrated in Figure 28. We have also examined the possible role of spall in explaining the anomalous late arrival of pP<sub>n</sub>.

We have already reported on interpretation of the majority of the available digitally recorded data from NTS. It would, of course, be desirable to analyze even more. After some investigation, we learned that regional data had been recorded for several decades by DOE on analog tape and a portion of it had been digitized with a high speed A to D converter. Figure 29 shows the locations of the stations which were operated for an extended period of time. Most of the instruments were L7s which are very broad band and, given the frequency of NTS testing, each recorded a substantial data base. Unfortunately, most of the stations are closer than P<sub>n</sub> cross over distance, so they can not be used to test the waveform discriminant directly. They do provide a significant data base for investigating other types of discriminants which are applicable at shorter ranges. The stations at Las Vegas are the most distant, and they are slightly beyond cross over range. The top of Figure 30 shows an enlarged map of the stations, and the bottom shows a seismic section of the P waves observed from the Yucca

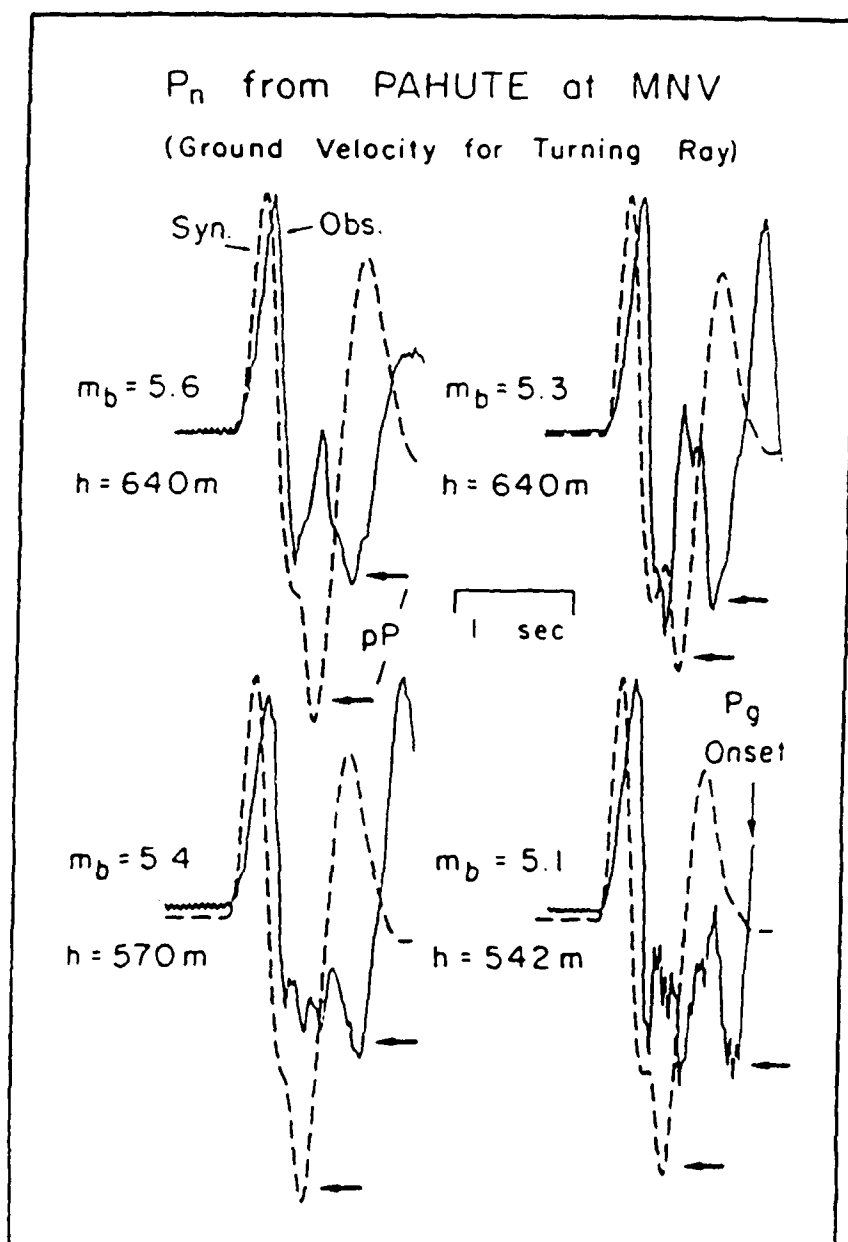


Figure 28. Observed versus synthetic  $P_n$  waveforms at MNV for Pahute events. The turning ray model for propagation is assumed. The Mueller-Murphy source scaling relations and a  $t^*$  value of 0.1 s are also assumed. As indicated by arrows, the observed  $pP$  arrival is late but approximately the same in size as the elastic prediction.

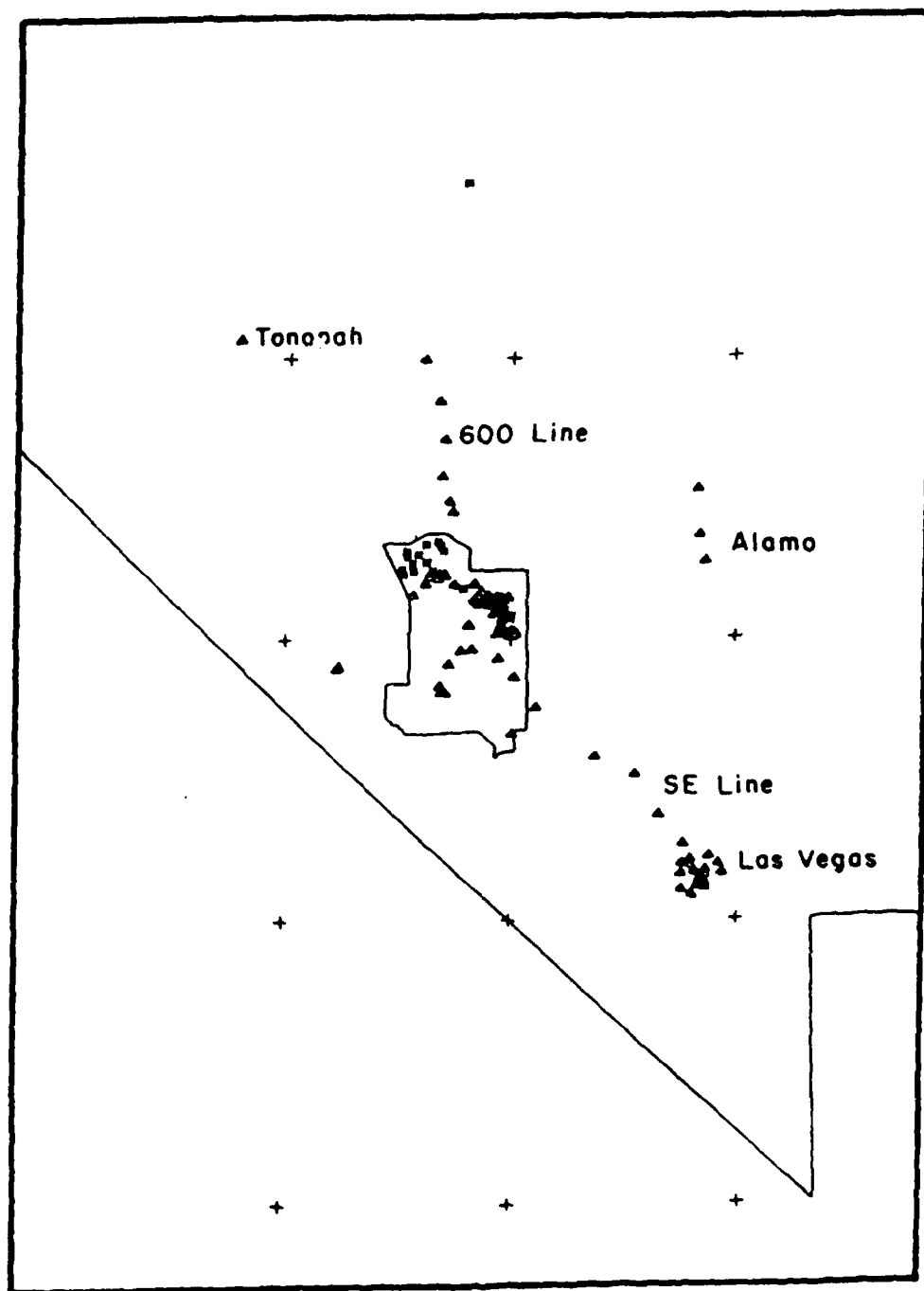


Figure 29. Map showing the locations of stations operated by DOE over an extended period of time.

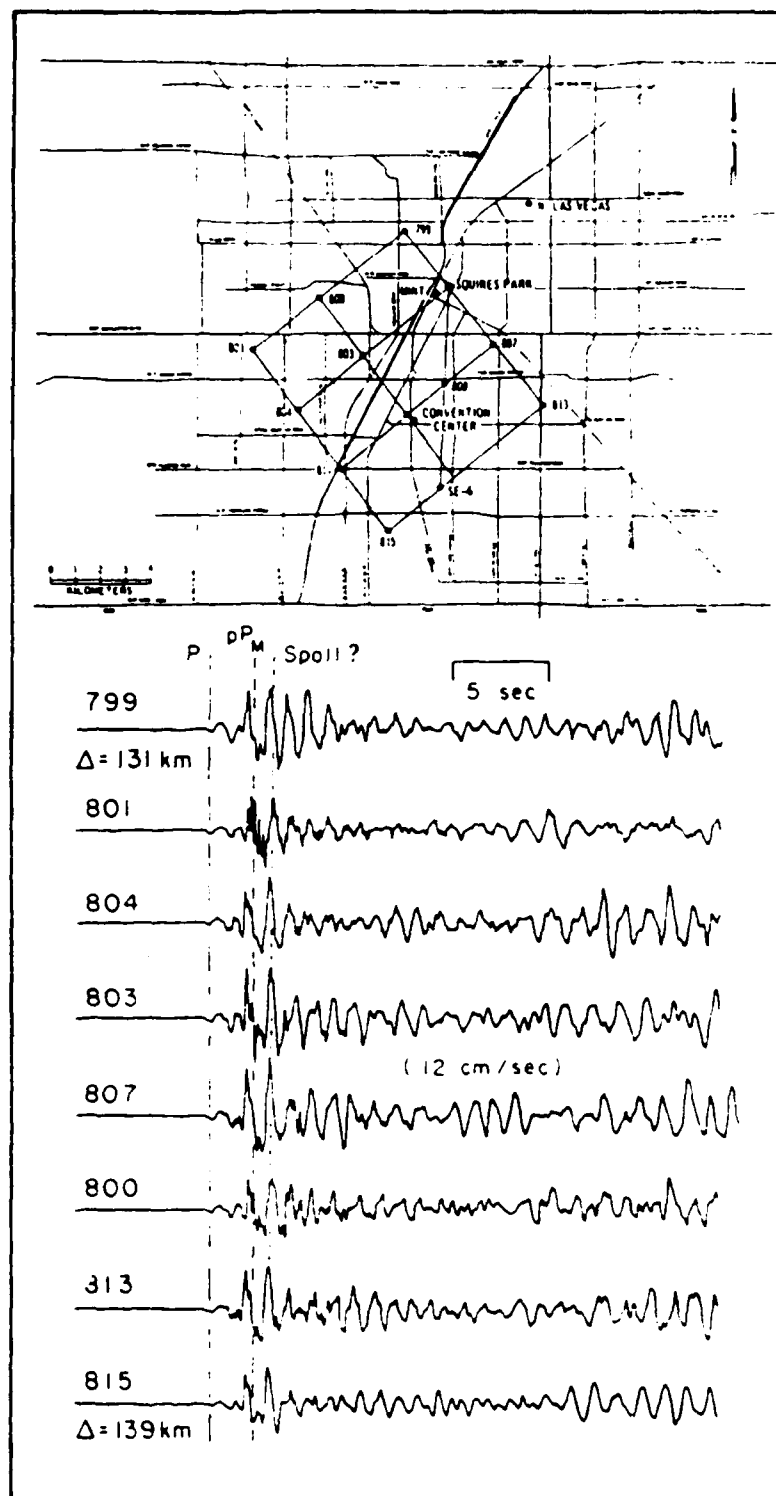


Figure 30. An enlarged map showing the locations of stations. Below is a seismic section of P waves observed from the Yucca event FLASK. The onsets of the waveforms are relatively stable.

event FLASK. The onset of the wave form appears relatively stable, and there is clear  $P_n$  moveout which is sufficient reason to attempt development of a crustal model.

We began our numerical experiments by attempting to use a layer over a half space model. Synthetics were computed with generalized ray theory. The travel times to Las Vegas constrained the model to be relatively slow. The speed of the mantle layer appeared to be only 7.9 km. If the travel time was matched by slowing the crustal layer, the contrast across the Moho became too large and the ratio of the head wave to the reflected energy was predicted to be too small. Introducing a gradient into the crust-mantle transition appears to be one of the best among several possible explanations. A transition zone of about 7 km, an average crustal speed of about 5.5 km/s and a mantle speed of 7.9 km/s appeared to fit the observations the best. Our preferred model is plotted in Figure 31.

Unfortunately, though the NTS-Las Vegas model fits the relative amplitude and timing of the data in Figure 30, it does not fit the later complexity. This was disappointing since after the initial 3 or 4 strong swings the later coda is relatively weak until the arrival of S. At this juncture, we decided to again draw on our experience from modeling teleseismic P to improve our physical understanding of  $P_n$ . The late arrival of  $pP_n$  (Figure 28) and the additional complexity in the compressional waveform corresponded exactly to features we had noted previously in teleseismic P. We had developed a theory and performed modeling experiments to show that these features could be explained relatively simply through the phenomenon of spall. We developed this model in working with the two Amchitka tests MILROW and CANNIKIN (Burdick et al., 1984).

Figure 32 shows the source representation we developed to represent the spalling process. We employed many of the ideas used in standard dislocation representations of earthquakes. As indicated in the Figure, the explosion itself

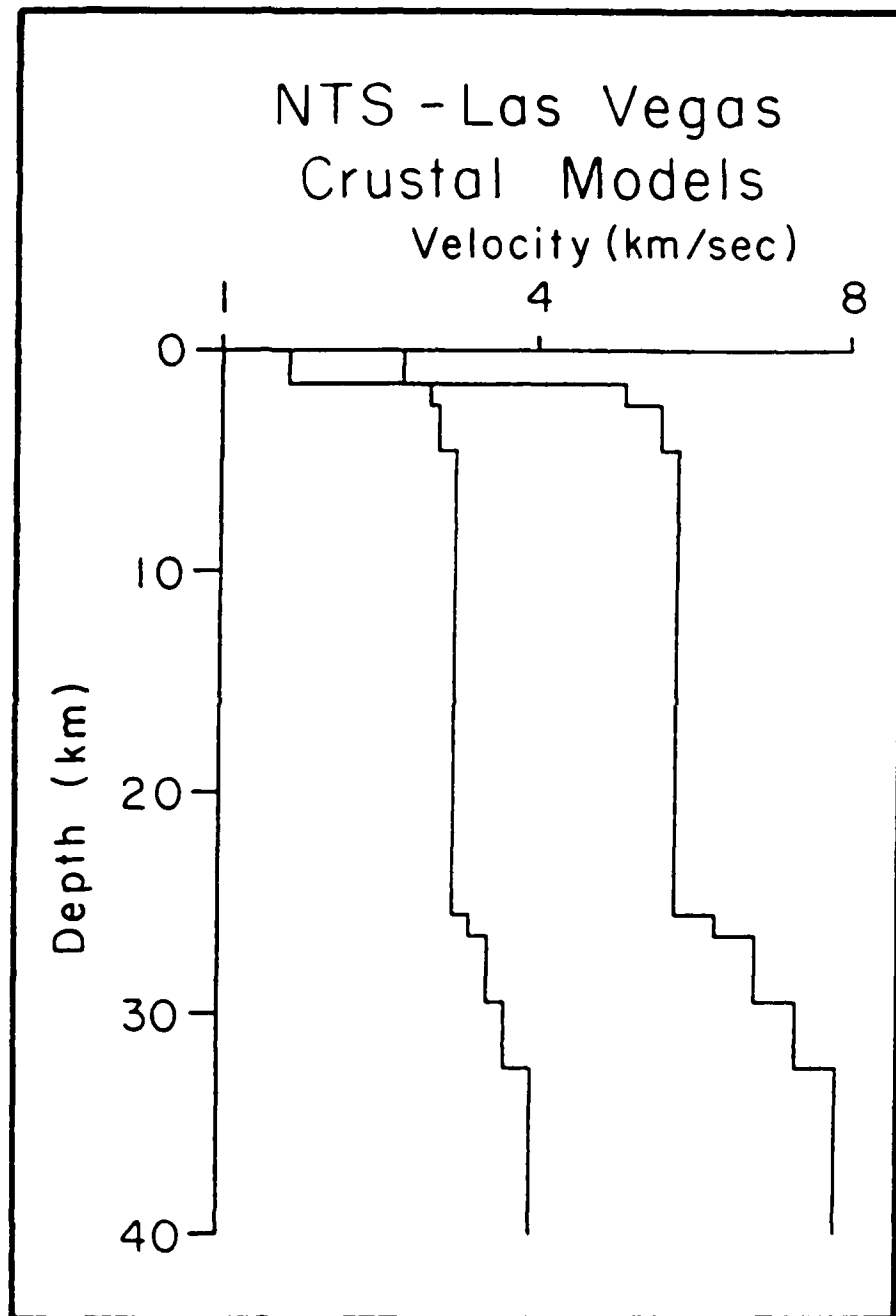


Figure 31. Preferred crustal model used to model the seismic section shown in Figure 30.

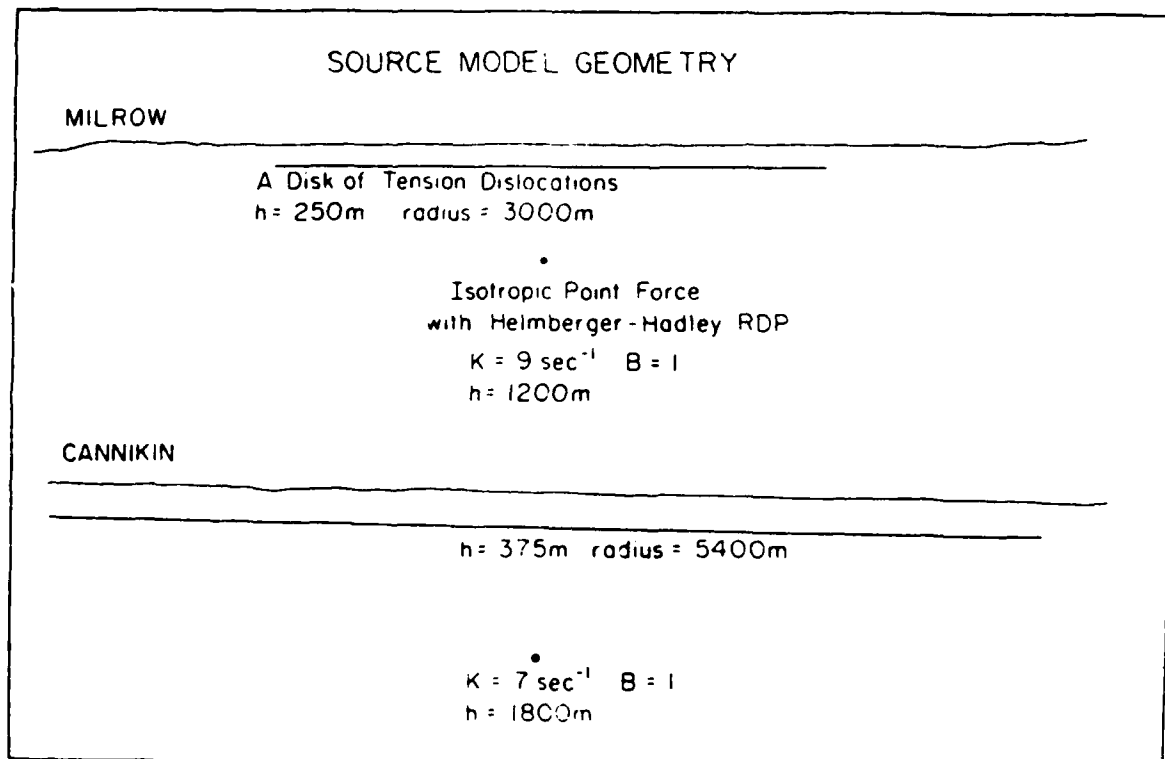


Figure 32. A scale drawing of the models for the explosion and spalling process. The explosion is itself an isotropic point source and the spall is represented by a shallow disk of tension dislocation.



is represented as an isotropic point force with an appropriate RDP as usual. We then represent a spall source as a shallow disk of tension dislocations. The dislocations are effectively replaced with a distribution of force systems just as an earthquake fault is replaced with a distribution of double couples. Tension dislocations can be expressed as a weighted sum of the basic double couples with the weight depending on the elastic constants of the medium. For the Amchitka tests, strong motion data were available from the spall zone from which we were able to specify the kinematics of motion on the tension dislocations. With this simple model and the relatively well constrained kinematics of motion we were able to explain the anomalies in the MILROW and CANNIKIN data.

Figure 33 illustrates in a simple way how the spall model can account for the observed delays in pP. As is well known, the spall crack opens when the tension from the downgoing surface reflected energy exceeds the compressions generated by the upgoing wave and the overburden pressure as well as the tensile strength of the containment medium. As this disk of tension dislocations begins to open, it radiates downward compressional energy coincident with the downgoing tension of pP. This is depicted in the first two rows of Figure 33. The pP and spall opening events will tend to cancel each other to some extent depending on the relative strength of the explosion and spall sources. The spall event removes energy from pP as one should expect. It also radiates compressional energy upward which reflects back into the earth as tension. This energy arrives after pP from the explosion with the same sign. It was our suggestion that this second spall phase was the phase that was being identified as a late arriving pP. As shown in the figure, there will also be a set of arrivals coming later associated with the spall closing event. These phases cause some complexities in the waveform that are in fact observed in the Amchitka data. The bottom trace in the figure shows the composite of the radiated pulses. Of course, the model is

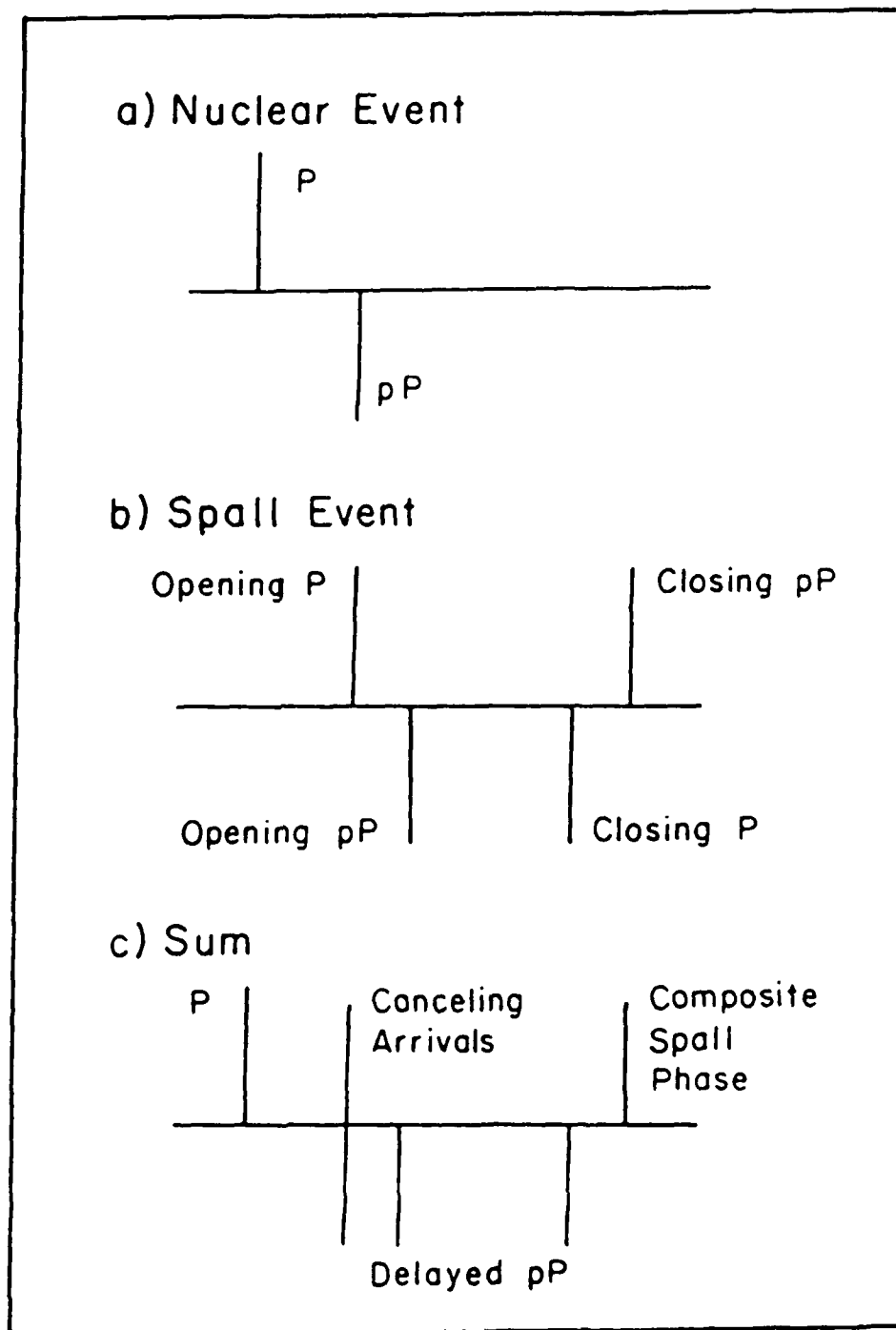


Figure 33. A model for the delay of  $pP$  by spall. The direct  $P$  and the  $pP$  arrivals are represented by spikes with appropriate polarity and arrival time. The delayed  $pP$  is actually the  $pP$  from spall opening and the spall arrival is a composite of the arrivals from the closing event.

very simplistic, but it does provide a framework in which we can at least begin to address the problem of the effects of spall. In the case of Amchitka, the free surface records indicated that the sizes of the explosion and spall sources were comparable, so this is an issue that needs to be addressed.

The results of our waveform modeling studies from which we developed the NTS to Las Vegas model in Figure 31 and of our spall modeling study are shown in Figure 34. Four representative P waveforms from Figure 30 are shown on the right. The  $P_n$  is small and emergent. The phase we have labeled as PmP is composed of several generalized rays just past critical angle in the lid gradient. The phase labeled pPmP is composed of the associated free surface reflected rays and they are of course opposite in sign. The first row of synthetics fits the observed waveforms for the first few oscillations, but there are consistently at least two continuing strong oscillations in the data which are not predicted. The center row of synthetics shows the effect of adding in the spall source. We estimated the delay of pP by spall at 0.3 seconds based on measurements from the deconvolved waveforms like those in Figure 28. The interference of the various arrivals was assumed to be as illustrated in Figure 33. The amplitude of the spall source was assumed to be equal to the explosion based on our Amchitka experience. The dwell time of the spall was adjusted to fit the data with a value of 0.3 seconds appearing to fit best. The match with the observations is good enough to suggest that spall is an important part of the explosion source which should be taken into account. The fact that a gradient model is required suggests that the P wave propagation to regional distances in the western U.S. can be best modeled with a continuous positive gradient (strong near the free surface) from the free surface down to the lid of the low velocity zone.

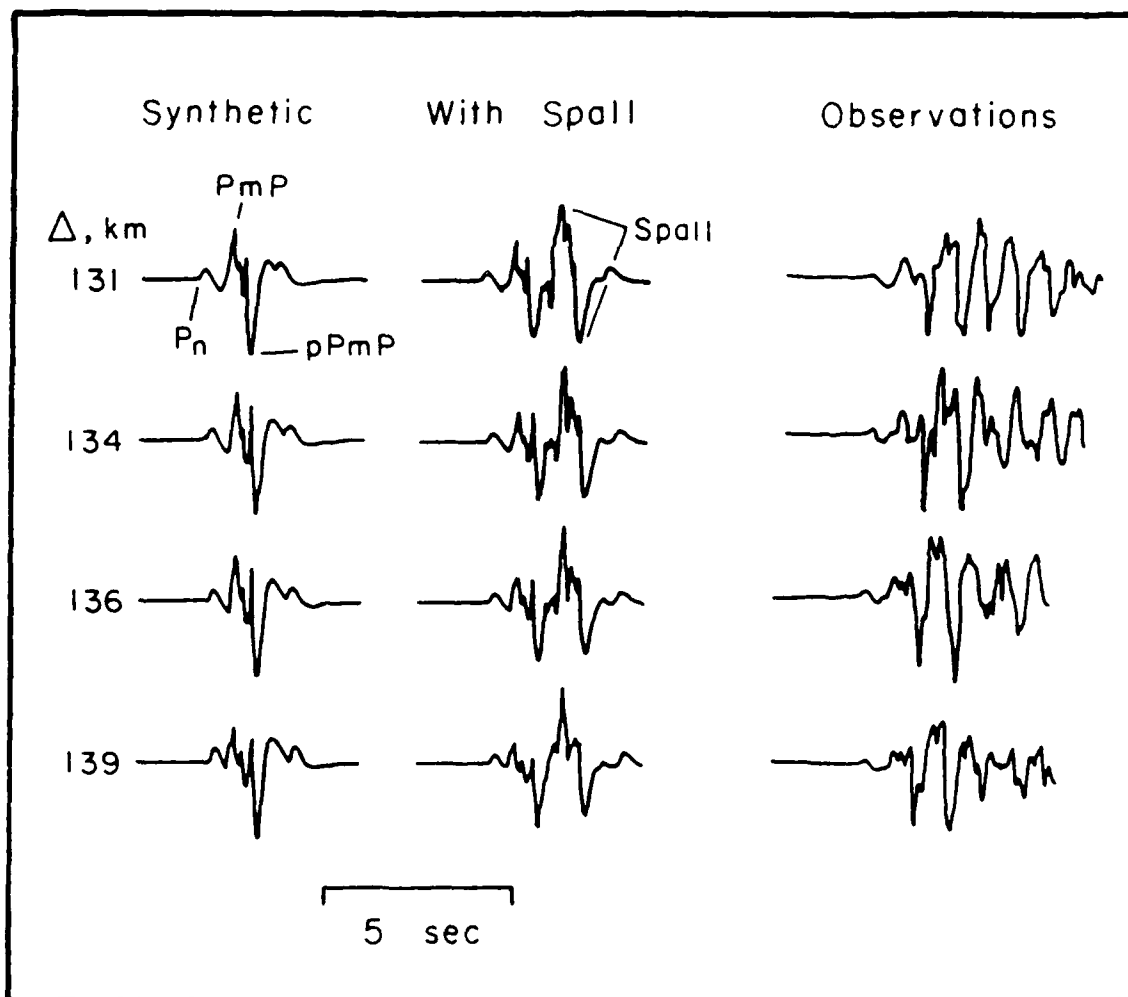


Figure 34. A comparison between the data and the synthetic seismograms. The synthetics on the left include the effects of the structure and an explosions source. Those in the center include the effects of spall. The data and the synthetics are in good agreement.

## CONCLUSIONS AND RECOMMENDATIONS

In overview, the most surprising and important result of this effort is that there is a great deal more organization and deterministic character in high frequency regional data than one might have expected from the review of previous work. There is no doubt that there is much scattering resulting in unstable high amplitude coda, but if one focuses on specific times in the records when wave propagation is simple to understand one can perform meaningful waveform modeling in the time domain. In this investigation we have worked with  $P_n$  and the onset of critical reflection from the Moho, but it seems likely that related approaches will work for tangential  $S_n$  and critical SH from the Moho.

Other more specific and new results have emerged from our efforts in developing numerical methods and performing numerical tests with them. We have developed wavenumber integration as a practical means of computing  $P_{n1}$  synthetics, though it requires judicious use of a Q model, damping through integration in the complex frequency plane and wavenumber filtering. We found that the results of the  $P_{n1}$  calculations do not depend strongly on the Q model, but it is numerically convenient to use one because it moves poles from the integration contour in the k plane. Our numerical tests showed conclusively that an appropriate model for the velocity gradients near the free surface is very significant to the accurate prediction of short period  $P_{n1}$ . Conversely, gradients near the crust model transition are not important to waveshape once the energy trapped there is well past critical. The fact that one simple layered model (our model 4) did a more than adequate job of explaining all of the observations from Pahute and Yucca is a strong indication that short period  $P_{n1}$  is a very stable and deterministic type of regional energy. This is promising for its future utility in solving the discrimination problem.

The progress in understanding the short period  $P_n$  waveform over the course of this investigation has been dramatic. Not only does it appear that the phase may provide the core of a physically based, transportable discriminant, but it also provides a new seismic window through which to observe the complex source process of nuclear event, spallation and tectonic release. These processes have been studied intensively over the last decades using teleseismic short period  $P$ . These investigations always seemed to produce inconclusive results because of trade offs between source processes and  $Q$ . It appears that almost nothing can be conclusively resolved if the possibility of laterally varying and strongly frequency dependent  $Q$  is considered. The average level of  $t^*$  appears to be of the order of 0.8 to 1.2 sec. which amounts to a very strong effect on the waveform. The level of  $t^*$  for  $P_n$  appears to be only about 0.1s; a drop of an order of magnitude in the attenuation exponential. This affords very definitive studies of the source processes. We strongly recommend further work on the short period  $P_n$  waveform discriminant in the future.

#### ACKNOWLEDGEMENTS

This relatively successful two year study could not have been carried out without the data from the western U.S. digital network which was generously provided by a number of individuals at several institutions. In particular, we would like to thank Dr. Steven Taylor at LLNL, Dr. Hiroo Kanamori at Caltech and Dr. Duncan Agnew at Scripps Institute.

## REFERENCES

- Aki, K. and P. G. Richards, "Quantitative Seismology - Theory and Methods", Vol-I  
W.H. Freeman and Company, 557p. 1980.
- Bouchon, M. "A simple method to calculate Green's functions for elastic layered  
media", Bull. Seis. Soc. Am., 71, 959-971 1981.
- Burdick L. J. and D. V. Helmberger, "The discrimination potential of crustal  
resonance phases", AFGL-TR-88-0054, Report 1, 73p, ADA196096, 1987.
- Burdick L. J., T. C. Wallace and T. X. Lay, "Modeling the near field and teleseismic  
observations from the Amchitka test site", J. Geophys. Res., 89, 4373-4388,  
1984.
- Burdick L. J., C. K. Saikia and N. F. Smith, "Discrimination using  $P_n$  and  $P_g$ ",  
AFGL-TR-88-0167, Report 2, 53p, ADA202018, 1988.
- Burdick, L. J., C. K. Saikia and N. F. Smith, " $P_n$  from the Nevada Test Site",  
AFGL-TR-89-0034, Report 3, 1988. ADA208276
- Dunkin, J. W., "Computation of modal solutions in layered, elastic media at  
high frequencies", Bull. Seis. Soc. Am., 55, 335-358, 1965.
- Harzell, S. H., L. J. Burdick and T. X. Lay, "Effective source functions for  
Pahute Mesa nuclear tests", Woodward Clyde Consultants Report, WCCP-83-03,  
Woodward Clyde Consultants, 566 El Dorado Street, Pasadena, CA, 91101, 1983.
- Haskell, N. A., "Radiation pattern of Surface waves from a point source in a  
multi-layered medium", Bull. Seis. Soc. Am., 54, 377-393, 1964.
- Helmberger, D. V., "On the structure of the low velocity zone of the low velocity  
zone", Geophys. J. R. A. Soc., 34, 251-263, 1973.
- Helmberger, D. V., "Long period body-wave propagation FROM 40° TO 130°", Bull.  
Seis. Soc. Am., 325-341, 1972.



- Helmberger, D. V. and G. R. Engen, "Modeling the long period body waves from shallow earthquakes at regional ranges", Bull. Seis. Soc. Am., 70, 1699-1714, 1980.
- Holt, W. E. and T. C. Wallace, "Crustal thickness and upper mantle velocities in the Tibetan Plateau Region from the inversion of Regional Pnl waveforms: Evidence for a thick upper mantle lid beneath southern Tibet", Geophys. J. Res., 1989 (in press).
- Kennett B. L. N, 1980. Seismic wave propagation in stratified media, Cambridge University Press., 342p.
- Lefevre, V. and D. V. Helmberger, "Variation in upper mantle P-wave velocity beneath north America (abstract), EOS, 65,234, 1984.
- Mallick S. and L. N. Frazer, "Practical aspects of reflectivity modeling", Geophysics, 1355-1364 1987.
- Mallick S. and L. N. Frazer, "Rapid computation of multioffset vertical seismic profile synthetic seismograms for layered media", Geophysics, 479-491, 1988.
- Murphy, J. R., 1971. Seismic source functions and magnitude determinations for underground nuclear detonation, Bull. Seis. Soc. Am., 67, 135-158.
- Murphy, J. R. and T. J. Bennett, "A discrimination analysis of short period regional seismic data recorded at the Tonto Forest Observatory", Bull. Seism. Soc. Am., 72, 1351-1366, 1982.
- Somerville, P. G., "Source-scaling relations of eastern north American earthquakes", Elect. Power Res. Inst. Report, 1986.
- Spudich, P. and U. Ascher, "Calculation of complete theoretical seismograms in vertically varying media using collocation methods", Geophy. R. A. Soc., 75, 101-124, 1983.

- Taylor, S.R., N. W. Sherman and M. D. Denny, "Spectral discrimination between NTS explosions and western United States earthquakes at regional distances". Bull. Seis. Soc. Am., 78, 1563-1579, 1988.
- Wang, C. Y. and R. B. Herrmann, "A numerical study of *P*, *SV* and *SH* wave generation in a plane layered medium", Bull. Seis. Soc. Am., 70, 1015-1036, 1980.
- Watson, T. H., "A note on fast computation of Rayleigh wave dispersion in the multi-layered elastic half space", Bull. Seis. Soc. Am., 60, 161-166, 1970.
- Wen, W. J., "Rayleigh wave attenuation in basin and range province", M.S. Thesis. Saint Louis University. 54p 1989.

CONTRACTORS (United States)

Professor Keiiti Aki  
Center for Earth Sciences  
University of Southern California  
University Park  
Los Angeles, CA 90089-0741

Professor Thomas Ahrens  
Seismological Lab, 252-21  
Div. of Geological & Planetary Sci.  
California Institute of Technology  
Pasadena, CA 91125

Professor Charles B. Archambeau  
Cooperative Institute for Resch  
in Environmental Sciences  
University of Colorado  
Boulder, CO 80309

Dr. Thomas C. Rache Jr.  
Science Applications Int'l Corp.  
10210 Campus Point Drive  
San Diego, CA 92121 (2 copies)

Dr. Muawia Barazangi  
Institute for the Study of  
of the Continent  
Cornell University  
Ithaca, NY 14853

Dr. Douglas R. Baumgardt  
Signal Analysis & Systems Div.  
ENSCO, Inc.  
5400 Port Royal Road  
Springfield, VA 22151-2388

Dr. Jonathan Berger  
IGPP, A-205  
Scripps Institution of Oceanography  
University of California, San Diego  
La Jolla, CA 92093

Dr. S. Bratt  
Science Applications Int'l Corp.  
10210 Campus Point Drive  
San Diego, CA 92121

Dr. Lawrence J. Burdick  
Woodward-Clyde Consultants  
P.O. Box 93245  
Pasadena, CA 91109-3245 (2 copies)

Professor Robert W. Clayton  
Seismological Laboratory/Div. of  
Geological & Planetary Sciences  
California Institute of Technology  
Pasadena, CA 91125

Dr Karl Coyner  
New England Research, Inc.  
76 Olcott Drive  
White River Junction, VT 05001

Dr. Vernon F. Cormier  
Department of Geology & Geophysics  
U-45, Room 207  
The University of Connecticut  
Storrs, Connecticut 06268

Dr. Steven Day  
Dept. of Geological Sciences  
San Diego State U.  
San Diego, CA 92182

Dr. Zoltan A. Der  
ENSCO, Inc.  
5400 Port Royal Road  
Springfield, VA 22151-2388

Professor John Ferguson  
Center for Lithospheric Studies  
The University of Texas at Dallas  
P.O. Box 830688  
Richardson, TX 75083-0688

Professor Stanley Flotte  
Applied Sciences Building  
University of California,  
Santa Cruz, CA 95064

Dr. Alexander Florence  
SRI International  
333 Ravenswood Avenue  
Menlo Park, CA 94025-3493

Professor Steven Grand  
University of Texas at Austin  
Dept of Geological Sciences  
Austin, TX 78713-7909

Dr. Henry L. Gray  
C.F. Frenshley Professor of Mathematics  
& Statistics, Vice Provost and Dean  
Department of Statistical Sciences  
Southern Methodist University  
Dallas, TX 75275

Professor Roy Greenfield  
Geosciences Department  
403 Deike Building  
The Pennsylvania State University  
University Park, PA 16802

Dr. Indra N. Gupta  
Teledyne Geotech  
314 Montgomery St.  
Alexandria, VA 22314

Professor David G. Harkrider  
Seismological Laboratory  
Div of Geological & Planetary Sciences  
California Institute of Technology  
Pasadena, CA 91125

Professor Donald V. Helmberger  
Seismological Laboratory  
Div of Geological & Planetary Sciences  
California Institute of Technology  
Pasadena, CA 91125

Professor Eugene Herrin  
Institute for the Study of Earth  
and Man/Geophysical Laboratory  
Southern Methodist University  
Dallas, TX 75275

Professor Robert B. Herrmann  
Department of Earth & Atmospheric  
Sciences  
Saint Louis University  
Saint Louis, MO 63156

Professor Bryan Isacks  
Cornell University  
Dept of Geological Sciences  
SNEE Hall  
Ithaca, NY 14850

Professor Lane R. Johnson  
Seismographic Station  
University of California  
Berkeley, CA 94720

Professor Thomas H. Jordan  
Department of Earth, Atmospheric  
and Planetary Sciences  
Mass Institute of Technology  
Cambridge, MA 02139

Dr. Alan Kafka  
Department of Geology &  
Geophysics  
Boston College  
Chestnut Hill, MA 02167

Professor Leon Knopoff  
University of California  
Institute of Geophysics  
& Planetary Physics  
Los Angeles, CA 90024

Professor Charles A. Langston  
Geosciences Department  
403 Deike Building  
The Pennsylvania State University  
University Park, PA 16802

Professor Thorne Lay  
Department of Geological Sciences  
1006 C.C. Little Building  
University of Michigan  
Ann Arbor, MI 48109-1063

Dr. Randolph Martin III  
New England Research, Inc.  
76 Olcott Drive  
White River Junction, VT 05001

Dr. Gary McCartor  
Mission Research Corp.  
735 State Street  
P.O. Drawer 719  
Santa Barbara, CA 93102 (2 copies)

Professor Thomas V. McEvilly  
Seismographic Station  
University of California  
Berkeley, CA 94720

Dr. Keith L. McLaughlin  
S-CUBED,  
A Division of Maxwell Laboratory  
P.O. Box 1620  
La Jolla, CA 92038-1620

Professor William Menke  
Lamont-Doherty Geological Observatory  
of Columbia University  
Palisades, NY 10964

Dr. Bernard Minster  
IGPP, A-205  
Scripps Institute of Oceanography  
Univ. of California, San Diego  
La Jolla, CA 92093

Professor Brian J. Mitchell  
Department of Earth & Atmospheric  
Sciences  
Saint Louis University  
Saint Louis, MO 63156

Mr. Jack Murphy  
S-CUBED, A Division of Maxwell Lab  
11800 Sunrise Valley Drive  
Suite 1212  
Reston, VA 22091 (2 copies)

Dr. Rao Nguyen  
GL/LWH  
Hanscom AFB, MA 01731-5000

Professor J. A. Orcutt  
IGPP, A-205  
Scripps Institute of Oceanography  
Univ. of California, San Diego  
La Jolla, CA 92093

Professor Keith Priestley  
University of Nevada  
Mackay School of Mines  
Reno, NV 89557

Professor Paul G. Richards  
Lamont-Doherty Geological  
Observatory of Columbia Univ.  
Palisades, NY 10964

Wilmer Rivers  
Teledyne Geotech  
314 Montgomery Street  
Alexandria, VA 22314

Dr. Alan S. Ryall, Jr.  
Center of Seismic Studies  
1300 North 17th Street  
Suite 1450

Arlington, VA 22209-2308 (4 copies)

Professor Charles G. Sammis  
Center for Earth Sciences  
University of Southern California  
University Park  
Los Angeles, CA 90089-0741

Professor Christopher H. Scholz  
Geological Sciences  
Lamont-Doherty Geological Observatory  
Palisades, NY 10964

Dr. Jeffrey L. Stevens  
S-CUBED,  
A Division of Maxwell Laboratory  
P.O. Box 1620  
La Jolla, CA 92038-1620

Professor Brian Stump  
Institute for the Study of Earth & Man  
Geophysical Laboratory  
Southern Methodist University  
Dallas, TX 75275

Professor Ta-Liang Teng  
Center for Earth Sciences  
University of Southern California  
University Park  
Los Angeles, CA 90089-0741

Dr. Clifford Thurber  
University of Wisconsin - Madison  
Dept. of Geology & Geophysics  
1215 West Dayton St.  
Madison, WI 53706

Professor M. Nafi Toksoz  
Earth Resources Lab  
Massachusetts Institute of Technology  
42 Carleton Street  
Cambridge, MA 02142

Professor Terry C. Wallace  
Department of Geosciences  
Building #77  
University of Arizona  
Tucson, AZ 85721

Weidlinger Associates  
ATTN: Dr. Gregory Wojcik  
4410 El Camino Real, Suite 110  
Los Altos, CA 94022

Ray Willeman  
GL/LWH  
Hanscom AFB, MA 01731-5000

Dr. Lorraine Wolfe  
GL/LWH  
Hanscom AFB, MA 01731-5000

Professor Francis T. Wu  
Department of Geological Sciences  
State University of New York  
at Binghamton  
Vestal, NY 13901

OTHERS (United States)

Dr. Monem Abdel-Gawad  
Rockwell Internat'l Science Center  
1049 Camino Dos Rios  
Thousand Oaks, CA 91360

Professor Shelton S. Alexander  
Geosciences Department  
403 Deike Building  
The Pennsylvania State University  
University Park, PA 16802

Dr. Ralph Archuleta  
Department of Geological Sciences  
Univ. of California at  
Santa Barbara  
Santa Barbara, CA

J. Barker  
Department of Geological Sciences  
State University of New York  
at Binghamton  
Vestal, NY 13901

Mr. William J. Best  
907 Westwood Drive  
Vienna, VA 22180

Dr. N. Biswas  
Geophysical Institute  
University of Alaska  
Fairbanks, AK 99701

Dr. G. A. Bollinger  
Department of Geological Sciences  
Virginia Polytechnical Institute  
21044 Derring Hall  
Blacksburg, VA 24061

Mr. Roy Burger  
1221 Serry Rd.  
Schenectady, NY 12309

Dr. Robert Burrige  
Schlumberger-Doll Resch Ctr.  
Old Quarry Road  
Ridgefield, CT 06877

Science Horizons, Inc.  
ATTN: Dr. Theodore Cherry  
710 Encinitas Blvd., Suite 200  
Encinitas, CA 92024 (2 copies)

Professor Jon F. Claerbout  
Professor Amos Nur  
Dept. of Geophysics  
Stanford University  
Stanford, CA 94305 (2 copies)

Dr. Anton W. Dainty  
Earth Resources Lab  
Massachusetts Institute of Technology  
42 Carleton Street  
Cambridge, MA 02142

Professor Adam Dziewonski  
Hoffman Laboratory  
Harvard University  
20 Oxford St.  
Cambridge, MA 02138

Professor John Ebel  
Dept of Geology and Geophysics  
Boston College  
Chestnut Hill, MA 02167

Dr. Donald Forsyth  
Dept of Geological Sciences  
Brown University  
Providence, RI 02912

Dr. Anthony Gangi  
Texas A&M University  
Department of Geophysics  
College Station, TX 77843

Dr. Freeman Gilbert  
Inst. of Geophysics & Planetary Physics  
University of California, San Diego  
P.O. Box 109  
La Jolla, CA 92037

Mr. Edward Giller  
Pacific Seirra Research Corp.  
1401 Wilson Boulevard  
Arlington, VA 22209

Dr. Jeffrey W. Given  
Sierra Geophysics  
11255 Kirkland Way  
Kirkland, WA 98033

Rong Song Jih  
Teledyne Geotech  
314 Montgomery Street  
Alexandria, VA 22314

Professor F.K. Lamb  
Univ. of Illinois at Urbana-Champaign  
Department of Physics  
1110 West Green Street  
Urbana, IL 61801

Dr. Arthur Lerner-Lam  
Lamont-Doherty Geological Observatory  
of Columbia University  
Palisades, NY 10964

Dr. L. Timothy Long  
School of Geophysical Sciences  
Georgia Institute of Technology  
Atlanta, GA 30332

Dr. Peter Malin  
University of California at  
Santa Barbara  
Institute for Central Studies  
Santa Barbara, CA 93106

Dr. George R. Mellman  
Sierra Geophysics  
11255 Kirkland Way  
Kirkland, WA 98033

Professor John Nabelek  
College of Oceanography  
Oregon State University  
Corvallis, OR 97331

Dr. Geza Nagy  
U. California, San Diego  
Dept of Ames, M.S. B-010  
La Jolla, CA 92093

Dr. Jack Oliver  
Department of Geology  
Cornell University  
Ithaca, NY 14850

Dr. Robert Phinney/Dr. F. A. Dahlen  
Dept of Geological  
Geological Science University  
Princeton University  
Princeton, NJ 08540

RADIX System, Inc.  
Attn: Dr. Jay Pulli  
2 Taft Court, Suite 203  
Rockville, Maryland 20850

Dr. Norton Rimer  
S-CUBED  
A Division of Maxwell Laboratory  
P.O. 1620  
La Jolla, CA 92038-1620

Professor Larry J. Ruff  
Department of Geological Sciences  
1006 C.C. Little Building  
University of Michigan  
Ann Arbor, MI 48109-1063

Dr. Richard Sailor  
TASC Inc.  
55 Walkers Brook Drive  
Reading, MA 01867

Thomas J. Sereno, Jr.  
Science Application Int'l Corp.  
10210 Campus Point Drive  
San Diego, CA 92121

Dr. David G. Simpson  
Lamont-Doherty Geological Observ.  
of Columbia University  
Palisades, NY 10964

Dr. Bob Smith  
Department of Geophysics  
University of Utah  
1400 East 2nd South  
Salt Lake City, UT 84112

Dr. S. W. Smith  
Geophysics Program  
University of Washington  
Seattle, WA 98195

Dr. Stewart Smith  
IRIS Inc.  
1616 N. Fort Myer Dr.  
Suite 1440  
Arlington, VA 22209

Rondout Associates  
ATTN: Dr. George Sutton,  
Dr. Jerry Carter, Dr. Paul Pomeroy  
P. O. Box 224  
Stone Ridge, NY 12484 (4 copies)

Dr. L. Sykes  
Lamont Doherty Geological Observ.  
Columbia University  
Palisades, NY 10964

Dr. Pradeep Talwani  
Department of Geological Sciences  
University of South Carolina  
Columbia, SC 29208

Dr. R. B. Tittmann  
Rockwell International Science Center  
1049 Camino Dos Rios  
P.O. Box 1085  
Thousand Oaks, CA 91360

Dr. Gregory van der Vink  
IRIS, Inc.  
1616 No. Fort Myer Drive  
Suite 1440  
Arlington, VA 22209

Professor John H. Woodhouse  
Hoffman Laboratory  
Harvard University  
20 Oxford St.  
Cambridge, MA 02138

Dr. Gregory B. Young  
ENSCO, Inc.  
5400 Port Royal Road  
Springfield, VA 22151-2388



FOREIGN (OTHERS)

Dr. Peter Basham  
Earth Physics Branch  
Geological Survey of Canada  
1 Observatory Crescent  
Ottawa, Ontario, CANADA K1A 0Y3

Professor Ari Ben-Menahem  
Dept of Applied Mathematics  
Weizman Institute of Science  
Rehovot  
ISRAEL 951729

Dr. Eduard Berg  
Institute of Geophysics  
University of Hawaii  
Honolulu, HI 96822

Dr. Michel Bouchon  
I.R.I.G.M.-B.P.  
38402 St. Martin D'Heres  
Cedex FRANCE

Dr. Hilmar Bungum/NTNF/NORSAR  
P.O. Box 51  
Norwegian Council of Science,  
Industry and Research, NORSAR  
N-2007 Kjeller, NORWAY

Dr. Michel Campillo  
I.R.I.G.M.-B.P. 68  
38402 St. Martin D'Heres  
Cedex, FRANCE

Dr. Kin-Yip Chun  
Geophysics Division  
Physics Department  
University of Toronto  
Ontario, CANADA M5S 1A7

Dr. Alan Douglas  
Ministry of Defense  
Blacknest, Brimpton,  
Reading RG7-4RS  
UNITED KINGDOM

Dr. Manfred Henger  
Fed. Inst. For Geosciences & Nat'l Res.  
Postfach 510153  
D-3000 Hannover 51  
FEDERAL REPUBLIC OF GERMANY

Ms. Eva Johannisson  
Senior Research Officer  
National Defense Research Inst.  
P.O. Box 27322  
S-102 54 Stockholm, SWEDEN

Tormod Kvaerna  
NTNF/NORSAR  
P.O. Box 51  
N-2007 Kjeller, NORWAY

Mr. Peter Marshall, Procurement  
Executive, Ministry of Defense  
Blacknest, Brimpton,  
Reading FG7-4RS  
UNITED KINGDOM (3 copies)

Dr. Robert North  
Geophysics Division  
Geological Survey of Canada  
1 Observatory crescent  
Ottawa, Ontario, CANADA K1A 0Y3

Dr. Frode Ringdal  
NTNF/NORSAR  
P.O. Box 51  
N-2007 Kjeller, NORWAY

Dr. Jorg Schlittenhardt  
Fed. Inst. for Geosciences & Nat'l Res.  
Postfach 510153  
D-3000 Hannover 51  
FEDERAL REPUBLIC OF GERMANY

University of Hawaii  
Institute of Geophysics  
ATTN: Dr. Daniel Walker  
Honolulu, HI 96822

FOREIGN CONTRACTORS

Dr. Ramon Cabre, S.J.  
Observatorio San Calixto  
Casilla 5939  
La Paz Bolivia

Professor Peter Harjes  
Institute for Geophysik  
Rhur University/Bochum  
P.O. Box 102148, 4630 Bochum 1  
FEDERAL REPUBLIC OF GERMANY

Dr. E. Husebye  
NTNF/NORSAR  
P.O. Box 51  
N-2007 Kjeller, NORWAY

Professor Brian L.N. Kennett  
Research School of Earth Sciences  
Institute of Advanced Studies  
G.P.O. Box 4  
Canberra 2601, AUSTRALIA

Dr. B. Massinon  
Societe Radiomana  
27, Rue Claude Bernard  
75005, Paris, FRANCE (2 copies)

Dr. Pierre Mechler  
Societe Radiomana  
27, Rue Claude Bernard  
75005, Paris, FRANCE

Dr. Svein Mykkeltveit  
NTNF/NORSAR  
P.O. Box 51  
N-2007 Kjeller, NORWAY (3 copies)

## GOVERNMENT

Dr. Ralph Alewine III  
DARPA/NMRO  
1400 Wilson Boulevard  
Arlington, VA 22209-2308

James C. Battis  
GL/LWH  
Hanscom AFB, MA 01731-5000

Dr. Robert Blandford  
DARPA/NMRO  
1400 Wilson Boulevard  
Arlington, VA 22209-2308

Dr. John J. Cipar  
GL/LWH  
Hanscom AFB, MA 01731-5000

Sandia National Laboratory  
ATTN: Dr. H. B. Durham  
Albuquerque, NM 87185

Dr. Jack Evernden  
USGS-Earthquake Studies  
345 Middlefield Road  
Menlo Park, CA 94025

U.S. Geological Survey  
ATTN: Dr. T. Hanks  
Nat'l Earthquake Resch Center  
345 Middlefield Road  
Menlo Park, CA 94025

Dr. James Hannon  
Lawrence Livermore Nat'l Lab.  
P.O. Box 808  
Livermore, CA 94550

Paul Johnson  
ESS-4, Mail Stop J979  
Los Alamos National Laboratory  
Los Alamos, NM 87545

Janet Johnston  
GL/LWH  
Hanscom AFB, MA 01731-5000

Dr. Katherine Kadinsky-Cade  
GL/LWH  
Hanscom AFB, MA 01731-5000

Ms. Ann Kerr  
IGPP, A-205  
Scripps Institute of Oceanography  
Univ. of California, San Diego  
La Jolla, CA 92093

Dr. Max Koontz  
US Dept of Energy/DP 5  
Forrestal Building  
1000 Independence Ave.  
Washington, D.C. 20585

Dr. W. H. K. Lee  
Office of Earthquakes, Volcanoes,  
& Engineering  
345 Middlefield Rd  
Menlo Park, CA 94025

Dr. William Leith  
U.S. Geological Survey  
Mail Stop 928  
Reston, VA 22092

Dr. Richard Lewis  
Dir. Earthquake Engrg & Geophysics  
U.S. Army Corps of Engineers  
Box 631  
Vicksburg, MS 39180

James F. Lewkewicz  
GL/LWH  
Hanscom AFB, MA 01731-5000

Stephen Mangino  
GL/LWH  
Hanscom AFB, MA 01731-5000

Dr. Robert Masse'  
Box 25046, Mail Stop 967  
Denver Federal Center  
Denver, CO 80225

Richard Morrow  
ACDA/VI  
Room 5741  
320 21st Street N.W.  
Washington, D.C. 20451

Dr. Keith K. Nakanishi  
Lawrence Livermore National Laboratory  
P.O. Box 808, L-205  
Livermore, CA 94550 (2 copies)

Dr. Carl Newton  
Los Alamos National Lab.  
P.O. Box 1663  
Mail Stop C335, Group ESS-3  
Los Alamos, NM 87545

Dr. Kenneth H. Olsen  
Los Alamos Scientific Lab.  
P.O. Box 1663  
Mail Stop C335, Group ESS-3  
Los Alamos, NM 87545

Howard J. Patton  
Lawrence Livermore National Laboratory  
P.O. Box 808, L-205  
Livermore, CA 94550

Mr. Chris Paine  
Office of Senator Kennedy  
SR 315  
United States Senate  
Washington, D.C. 20510

AFOSR/NP  
ATTN: Colonel Jerry J. Perrizo  
Bldg 410  
Rolling AFB, Wash D.C. 20332-6448

HQ AFTAC/TT  
Attn: Dr. Frank F. Pilotte  
Patrick AFB, Florida 32925-6001

Mr. Jack Rachlin  
USGS - Geology, Rm 3 C136  
Mail Stop 928 National Center  
Reston, VA 22092

Robert Reinke  
AFWL/NTEG  
Kirtland AFB, NM 87117-6008

Dr. Byron Ristvet  
HQ DNA, Nevada Operations Office  
Attn: NVCG  
P.O. Box 98539  
Las Vegas, NV 89193

HQ AFTAC/TGR  
Attn: Dr. George H. Rothe  
Patrick AFB, Florida 32925-6001

Donald L. Springer  
Lawrence Livermore National Laboratory  
P.O. Box 808, L-205  
Livermore, CA 94550

Dr. Lawrence Turnbull  
OSWR/NED  
Central Intelligence Agency  
CIA, Room 5G48  
Washington, D.C. 20505

Dr. Thomas Weaver  
Los Alamos National Laboratory  
P.O. Box 1663  
MS C 335  
Los Alamos, NM 87545

GL/SULL  
Research Library  
Hanscom AFB, MA 01731-5000 (2 copies)

Secretary of the Air Force (SAFRD)  
Washington, DC 20330  
Office of the Secretary Defense  
DDR & E  
Washington, DC 20330

HQ DNA  
ATTN: Technical Library  
Washington, DC 20305

DARPA/RMO/RETRIEVAL  
1400 Wilson Blvd.  
Arlington, VA 22209

DARPA/RMO/Security Office  
1400 Wilson Blvd.  
Arlington, VA 22209

GL/XO  
Hanscom AFB, MA 01731-5000

GL/LW  
Hanscom AFB, MA 01731-5000

DARPA/PM  
1400 Wilson Boulevard  
Arlington, VA 22209

Defense Technical  
Information Center  
Cameron Station  
Alexandria, VA 22314  
(5 copies)

Defense Intelligence Agency  
Directorate for Scientific &  
Technical Intelligence  
Washington, D.C. 20301

Defense Nuclear Agency/SPSS  
ATTN: Dr. Michael Shore  
6801 Telegraph Road  
Alexandria, VA 22310

AFTAC/CA (STINFO)  
Patrick AFB, FL 32925-6001

Mr. Alfred Lieberman  
ACDA/VI-OA'State Department Building  
Room 5726  
320 - 21st Street, NW  
Washington, D.C. 20451

TACTEC  
Rattelle Memorial Institute  
505 King Avenue  
Columbus, OH 43201 (Final report only)